NASA Contractor Report 4619

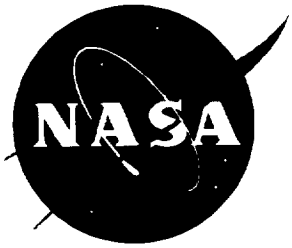

Venusian Atmospheric and Magellan Properties From Attitude Control Data

Christopher A. Croom and Robert H. Tolson
The George Washington University, Joint Institute for Advancement of Flight Sciences,
Langley Research Center • Hampton, Virginia

National Aeronautics and Space Administration
Langley Research Center • Hampton, Virginia 23681-0001

Prepared for Langley Research Center
under Cooperative Agreement NCC1-104

August 1994

Abstract

Results are presented of the study of the Venusian atmosphere, Magellan aerodynamic moment coefficients, moments of inertia, and solar moment coefficients. This investigation is based upon the use of attitude control data in the form of reaction wheel speeds from the Magellan spacecraft. As the spacecraft enters the upper atmosphere of Venus, measurable torques are experienced due to aerodynamic effects. Solar and gravity gradient effects also cause additional torques throughout the orbit. In order to maintain an inertially fixed attitude, the control system counteracts these torques by changing the angular rates of three reaction wheels. Model reaction wheel speeds are compared to observed Magellan reaction wheel speeds through a differential correction procedure.

This method determines aerodynamic, atmospheric, solar pressure and mass moments of inertia parameters. Atmospheric measurements include both base densities and scale heights. Atmospheric base density results confirm natural variability as measured by the standard orbital decay method. Potential inconsistencies in free molecular aerodynamic moment coefficients are identified. Moments of inertia are determined with a precision better than 1% of the largest principal moment of inertia.

Table of Contents

List of Figures

List of Tables

Nomenclature

a	solar array width, m
A	sensitivity matrix
A_a	reference area for atmospheric torque, m^2
A_s	reference area for solar torque, m^2
$A_n^T \Gamma_\epsilon^{-1} A_n$	information matrix
b	solar array length, m
c_{md}	aerodynamic moment coefficient
c_{ms}	solar moment coefficient
C	constant
g	gravitational acceleration, m/s^2
h	altitude, km
h_o	base altitude, km
H	angular momentum, $kg \cdot m^2/s$
H_s	scale height, km
$\vec{i}, \vec{j}, \vec{k}$	unit vectors in spacecraft coordinate system
I_{ij}	spacecraft mass moment of inertia, $kg \cdot m^2$
I_{rw}	reaction wheel moment of inertia for axis of rotation, $kg \cdot m^2$
J	cost function
l, m, n	direction cosines
L_a	reference length for aerodynamic torque, m
L_s	reference length for solar torque, m
m	solar array mass, kg
m_H	atmospheric atomic mass

M	number of parameters
n	iteration number
N	number of data points
p	solar momentum flux, kg/(m·s^2)
P	generic parameter
R	spacecraft radial distance from Venus center of attraction, m
R^*	universal gas constant, kJ/(kgmol·K)
t	time index
T	environmental torque, N·m
T_a	atmospheric torque, N·m
T_g	gravity gradient torque, N·m
T_s	solar pressure torque, N·m
T_H	atmospheric temperature, °K
v	spacecraft velocity, m/s
$\vec{x}$	parameter state vector
x_c, y_c, z_c	center of mass location in spacecraft coordinates, m
$\vec{y}$	observed reaction wheel speed, rad/sec
α	scale height correction factor
β	angle between roll axis and solar array surface, degrees
Γ_x	a priori covariance matrix
Γ_ε	measurement covariance matrix
$\vec{\varepsilon}$	residuals, rad/sec
θ	angle between roll axis and active solar array normal, degrees
$\vec{\mu}_x$	a priori estimates
μ	Venus gravitational constant, m^3/s^2
ρ	atmospheric density, kg/m^3

ρ_o	atmospheric base density, kg/m^3
σ_ε	measurement standard deviation
σ_x	a priori standard deviation
ω	model reaction wheel speed, rad/sec

Abbreviations

AACS	Attitude and Articulation Control System
ARU	Attitude Reference Unit
Freemac	Free molecular flow simulation software
LST	Local Solar Time
MACDAS	Magellan Attitude Control Data Analysis Software
VIRA	Venus International Reference Atmosphere

I. INTRODUCTION

I.1 Purpose of Study

The purpose of this research is to develop an alternate technique to the standard orbital decay method[1] to determine Venusian atmospheric densities. This technique was used to confirm the large natural variability in atmospheric density observed by the orbital decay measurements prior to the Magellan aerobraking experiment[2,3]. In addition to density, atmospheric scale heights, spacecraft aerodynamic moment coefficients, solar moment coefficients, and mass moments of inertia are also determined. This technique uses attitude control data from the Magellan spacecraft in the form of reaction wheel speeds. This work is a continuation of a feasibility study done by Marsden and Croom[4,5] and extends results presented by Croom and Tolson[6].

The reaction wheel method presents several advantages to the orbital decay method of determining atmospheric densities. This orbital decay method is based on the use of Doppler shift measurements. Using reaction wheel data eliminates the "plane of sky" problem inherent in Doppler shift measurements, and has the ability to determine spatial atmospheric variation on each orbit. For one orbit, the decay method is limited to base density determination whereas the reaction wheel data contains density variation information that represents scale heights and/or latitudinal variation. Since the Magellan spacecraft does not have the ability to record reaction wheel speeds, all data must be transmitted to Earth as it is observed. On the other hand, Doppler results can be obtained without spacecraft communication at periapsis.

I.2 Previous Work

This research relies upon previous study of the Venusian atmosphere using drag data obtained from the Pioneer-Venus mission. This data was used as the basis for the Venus International Reference Atmosphere (VIRA).[7]

This work also required Magellan spacecraft mass moment of inertia values that were obtained from an in-flight calibration performed by Martin Marietta (Personal communication, H. Curtis, Martin Marietta Corporation, March 31, 1993).

I.3 Report Organization

This report is organized into eight sections. The first section includes an introduction to the problem addressed. The second section describes the Magellan spacecraft - the vehicle used to obtain all data. Section III documents the mathematical model proposed to predict Magellan reaction wheel speed, while section IV describes the differential correction scheme used to determine model parameters. Sections V and VI present, respectively, parameter and parameter accuracy results. Section VII outlines conclusions and section VIII suggests future research on this topic.

II. MAGELLAN SPACECRAFT

II.1 Vehicle Description

II.1.1 Spacecraft

Magellan was built Martin Marietta Astronautics Group in Denver, Colorado. Figure 1.1 shows the Magellan spacecraft and the body-fixed coordinate system.

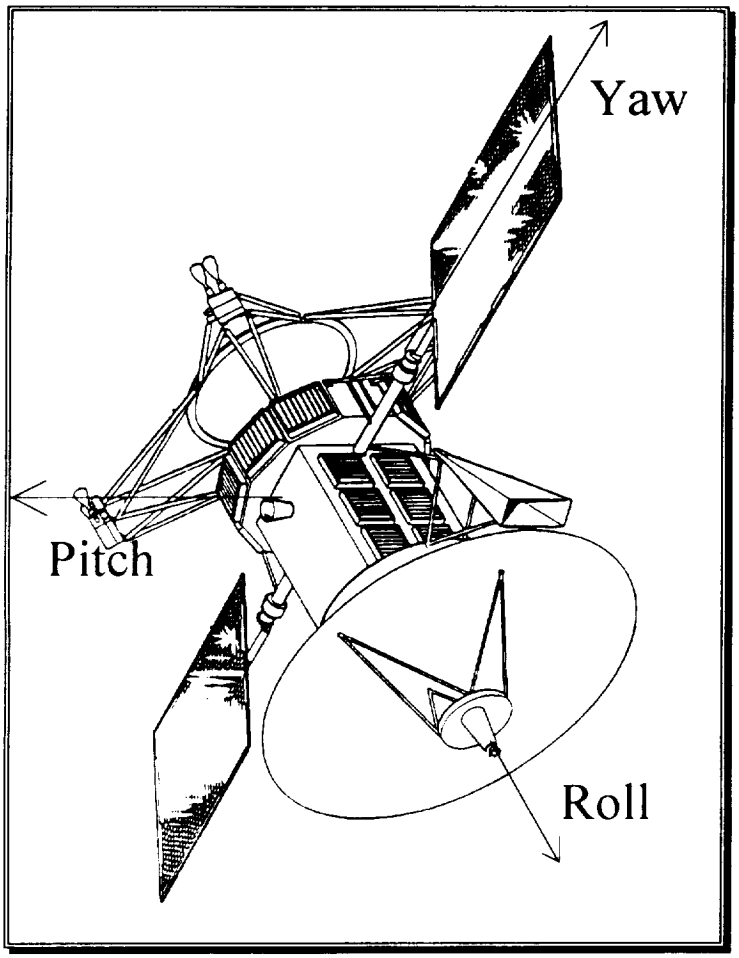

Figure 1.1 The Magellan Body-Fixed Coordinate System

The roll direction is defined by a vector pointing in the nominal direction of the high gain antenna boresight. The yaw axis is coincident with the solar array axis of rotation. The positive sense of this direction is defined by the spacecraft side with the altimeter antenna. The pitch axis completes a yaw, pitch, roll, right-handed system. A reaction wheel is located along each of these three directions. Under normal conditions, the roll axis points to Earth. The spacecraft is then rolled so that the yaw axis is normal to the spacecraft-sun line. Finally, the solar arrays are rotated about the yaw axis so as to be normal to the spacecraft-sun line. This specification uniquely determines the attitude of the spacecraft and solar array position at periapsis. Under this configuration, the spacecraft velocity vector is generally within 15° of the yaw axis at periapsis. During a large portion of Cycle

large portion of Cycle Four, a 10° Earth-point roll was implemented (i.e., spacecraft is rotated +10° about the roll axis) for mission thermal constraints. An x-y-z system is also used such that +x coincides with Yaw, +y is Pitch, and +z is Roll.

II.1.2 Attitude and Articulation Control System

Magellan attitude is controlled by the Attitude and Articulation Control System (AACS). The AACS maintains the inertially fixed attitude, described in section I.4, during periapsis and points the spacecraft in any required direction as dictated by mission requirements. Attitude adjustments are necessary for mapping, communications, star tracker scans, and momentum desaturations. The spacecraft is 3-axis stabilized by both reaction control thrusters and reaction wheels. Since only reaction wheels are used during periapsis events of Cycle Four, only that attitude control data is relevant to this study.

Attitude is measured by gyroscopes within the Attitude Reference Unit (ARU). This attitude is updated by a star tracker scan on each orbit and is recorded by a set of four Euler parameters, or quaternions. These quaternions uniquely define spacecraft attitude referenced to the J2000 inertial reference frame.[8] Quaternions are used to calculate the transformation matrix necessary to convert coordinates from the J2000 system into the Magellan body-fixed coordinate system with no physical singularities.[9]

II.1.3 Reaction Wheels

By changing the speed of the reaction wheels, the AACS controls the angular momentum of the spacecraft. By conservation of angular momentum (in the absence of external torques) changes in the speed of these wheels must be accompanied by changes in spacecraft angular rates. In this manner, Magellan attitude and angular rates are controlled. In a similar fashion, when the spacecraft experiences environmental torques,

AACS must change the angular rates of the reaction wheels in order to maintain an inertially fixed attitude. Angular momentum is thus transferred and stored within the reaction wheels. This angular momentum is removed from the reaction wheels during desaturation maneuvers. During these desaturation maneuvers, thrusters are used to exert a net moment on the spacecraft such that the reaction wheels must slow down in order to counteract the thruster moment. Reaction wheel specifications are give in Table 2.1 (Personal communication, Mike Nicholas, Honeywell Satellite Systems, Inc., March 16, 1993).

Stiction	< 0.01 N·m
Maximum Angular Rate	470 rad/s
Maximum Torque Output	0.18 N·m
Measurement Quantization	1.0236 rad/s/bit
Principal Moment of Inertia	0.06638 kg·m^2
Maximum Momentum Storage	27.0 N·m·s
Maximum (Peak) Power Usage	145 W
Time to Switch Torque Direction	< 0.1 s

Table 2.1 Reaction Wheel Specifications

II.1.4 Tachometers

Two redundant tachometers are used to measure the speed of each reaction wheel. These devices rely on Hall effect sensors and commutators. Measurement of wheel speed is quantized to 1.0236 rad/s/bit by the tachometers. The sensors detect changes in the

local magnetic field caused by the passing commutator and can therefore determine the angular velocity of the reaction wheel.

Although speed is quantized to 1.0236 rad/s/bit, the noise level of the measurement signal may be much larger. At low reaction wheel speeds, measurements tend to lie within a range of ± 2.6 rad/s. This is much larger than the range of ± 0.5118 rad/s that the reaction wheel demonstrates at higher speeds. This anomaly is attributed to "stiction" or "dynamic friction" within the reaction wheel assembly.

II.2 Mission Description

The Magellan spacecraft was launched from the space shuttle Atlantis, STS-30, on May 4, 1989. After reaching Venus in August of 1990, the primary mission of mapping the planet surface continued for three Venusian sidereal days. Over 97% of the planet's surface was mapped through the use of synthetic aperture radar.[10] September 15, 1992, marked the beginning of Cycle Four, the fourth sidereal day, which was reserved for gravitation field analysis. In addition, atmospheric studies were included to confirm atmospheric and aerodynamic properties prior to aerobraking. A series of aerobraking maneuvers was executed at the conclusion of Cycle Four to circularize the Magellan orbit. This new orbit would allow greater resolution in gravity measurements near the Venus poles.[11]

II.3 Orbit Description

During Cycle Four, Magellan was in a nearly polar orbit with an eccentricity of 0.39. Periapsis altitude ranged from 165 km to 185 km and the orbital period was 3.25 hours. Argument of periapsis and longitude of the ascending node were such that the spacecraft approached periapsis, which occurred at approximately 11° north latitude,

from the Venus North Pole. Under these conditions, atmospheric torques are detectable by the control system for up to 200 seconds during the periapsis event. The first orbit of Cycle Four was orbit #5754 that occurred on September 15, 1992, and the final orbit was orbit #7626 that occurred on May 26, 1993. This study represent a complete analysis of Cycle Four. (See Appendix E for more complete history of spacecraft orbit, configuration, and geometry during Cycle Four.)

II.4 Data Requirements

Data required for reaction wheel analysis consists of tachometer speeds, quaternions, and Magellan orbital elements. Orbital elements include semimajor axis, eccentricity, inclination, longitude of the ascending node, argument of periapsis, and time of periapsis. Reaction wheel speeds and spacecraft attitude are transmitted from the spacecraft at either a high or low data rate. For high rate data, reaction wheel speed has a sample period of 0.667 seconds. In the case of low rate, the sample period is 20 seconds (see Appendix E, Figure E.15). High rate transmission is preferable, but not always available due to mission constraints. In general, reaction wheel speeds and quaternions are transmitted for a period of time corresponding to twenty minutes before and after periapsis. The spacecraft attitude can be assumed to be inertially fixed during this time since the quaternions show no change in the four decimal places recorded by the AACS. Thus it can be assumed that all net change in spacecraft angular momentum, which is caused by external torques, is absorbed by the reaction wheels.

Orbital elements are determined from tracking data and an orbit determination algorithm. The classical orbital elements including time of periapsis are determined for each orbit. This information is required for orbit simulation.

In order for the reaction wheel method to be implemented, all of the above described data must be available. Further, the effectiveness of this method is affected by

the quantity of reaction wheel data available for a given orbit. For example, scale height measurements require data to be transmitted at the high rate, while mass moment of inertia and solar pressure parameters call for data to extend well beyond the atmospheric flight phase.

III. REACTION WHEEL SPEED MODEL

III.1 Introduction

In this section, a model for parameter estimation will be postulated and examined using prior information about the environmental torques and Magellan spacecraft.

Modeled reaction wheel speeds can be compared to observed reaction wheel speeds in order to determine environmental torques experienced by the Magellan spacecraft. Modeling reaction wheel speed requires the modeling of all significant torques and the parameterizing of these models. Significant torques experienced by the spacecraft are caused by aerodynamic forces, gravity gradients, and solar pressure forces. Modeling torques caused by these three physical phenomenon will provide an estimate of the total torque experienced by the spacecraft during a specified time interval. Reaction wheel speeds are a corollary of these total torques as given by the following equation (see appendix A).

$$\omega = \frac{1}{I_{rw}} \int T dt + C \qquad (1)$$

III.2 Atmospheric / Aerodynamic Torques

Aerodynamic forces are experienced by Magellan as it enters the Venusian upper atmosphere. Dynamic pressure at periapsis may approach $1.7 \cdot 10^{-4}\ N/m^2$. Depending upon spacecraft configuration and relative wind direction, an offset exists between the center of aerodynamic pressure and spacecraft center of mass. This offset results in a moment, or torque, due to atmospheric dynamic pressure. Maximum torque caused by the Venusian atmosphere during Cycle Four was approximately $1.6 \cdot 10^{-3}\ N \cdot m$. Aerodynamic torque can be resolved into the three body-fixed axes: yaw, pitch, and roll. Each component of torque due to atmospheric effects is determined by the relation

$$T_a = \frac{1}{2} v^2 c_{md} \rho A_a L_a \qquad (2)$$

where v is determined from the solution of the two-body problem and ρ is density. A_a and L_a are defined, respectively, as characteristic area (23 m^2) and length (3.66 m). The unknowns are therefore the aerodynamic moment coefficients c_{md} and the atmospheric base density. For mission operations, c_{md} is determined from a free molecular flow simulation (Freemac)[12] and ρ is obtained from the Venusian International Reference Atmosphere (VIRA). For scientific purposes, ρ is considered unknown. On the other hand, if ρ were known, then three aerodynamic moment coefficients could be determined since Eq. (2) applies to three independent coordinate axes: yaw, pitch, and roll. Accordingly, there are three unknown aerodynamic moment coefficients and one unknown base density. Variation in density near periapsis is modeled through the use of a piecewise continuous exponential function that matches VIRA densities at five kilometer intervals. Between these points, density is modeled as

$$\rho = \rho_{o} e^{\left(\frac{h-h_{o}}{H}\right)} \qquad (3)$$

where scale height can be related to atmospheric temperature by $H_{s} \equiv R^{*} T_{n} / m_{n} g$. The atmosphere is therefore divided into five kilometer layers. Within each layer, scale height is assumed constant. A general, simplified atmospheric structure can then be described by a base density at some altitude and a set of scale heights above the base altitude. Both density and scale heights are functions of altitude and local solar time as shown in Figures 3.1 and 3.2.

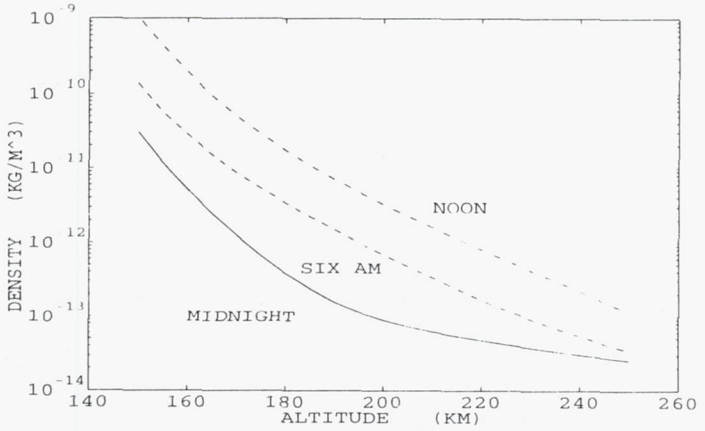

Figure 3.1 VIRA Density at Three Local Solar Times

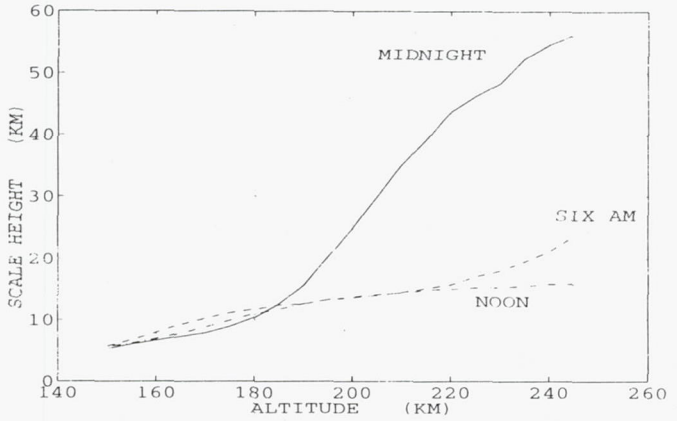

Figure 3.2 VIRA Scale Heights at Three Local Solar Times

Finally, change in reaction wheel speed due to atmospheric torques is determined by an integration of atmospheric torques. An example change in speed of the three reaction wheels due to aerodynamic phenomenon is shown in Figure 3.3.

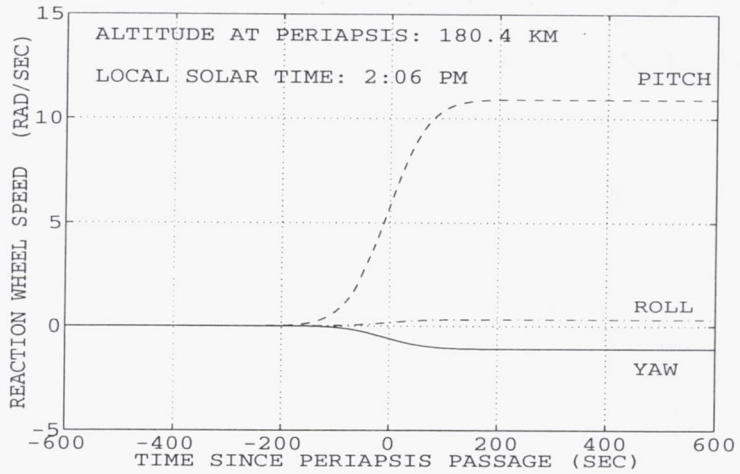

Figure 3.3 Reaction Wheel Speed Due to Atmospheric Torque

An inherent difficulty of this procedure is isolating the moment coefficient parameters and base density. This can be attributed to the fact that these parameters always appear together as a product. In order to solve this problem, some type of flow simulation must be performed to determine at least one aerodynamic moment coefficient. Once one of the three moment coefficients is known, base density and the remaining two aerodynamic coefficients can be estimated from the data. Accurate moment coefficient determination is computationally expensive. Limited free molecular flow simulations have been completed by Martin Marietta Corporation (Personal communication, B. Willcockson, Martin Marietta Corporation, March 30, 1993, and M. Patterson, Martin Marietta Corporation, February 20, 1994). Interpolation between completed Freemac simulations is used for missing moment coefficients. In Figures 3.4 and 3.5, pitch moment coefficients as determined by Freemac simulations are indicated by circles. A

sign change in the pitch aerodynamic moment coefficient occurs near inferior conjunction when the spacecraft executes a 180° roll maneuver. For purposes of presentation, these coefficients are plotted separately for periods before and after conjunction. Solid lines indicate the interpolation scheme. Discontinuities appear as the result of either spacecraft rolls or solar array off-point adjustments to satisfy mission thermal constraints (see Appendix E, Figure E.15).

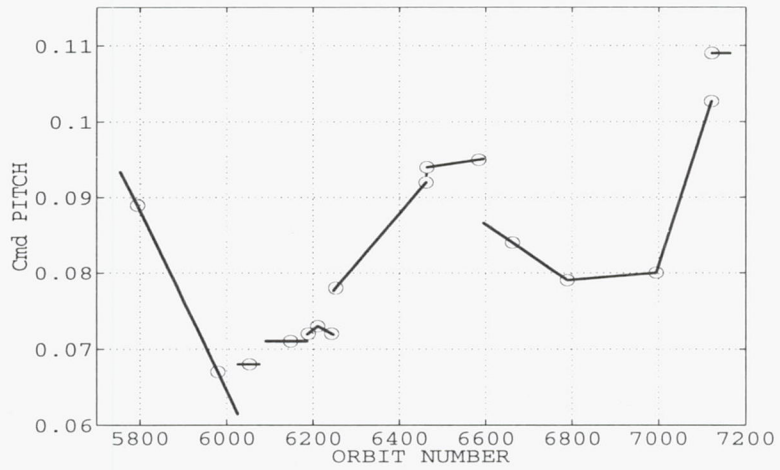

Figure 3.4 Freemac Pitch Aerodynamic Moment Coefficients (Before Conjunction)

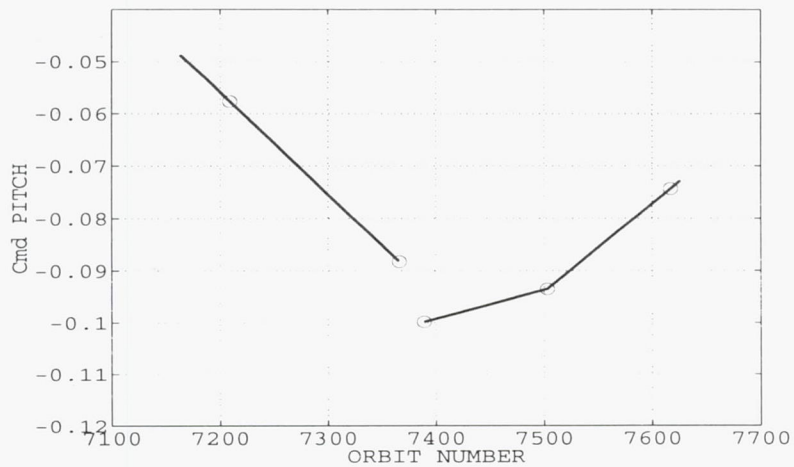

Figure 3.5 Freemac Pitch Aerodynamic Moment Coefficients (After Conjunction)

Reaction wheel data also provides the ability to determine scale heights. To parameterize the model, a correction factor α is introduced. This modifies the density equation as follows

$$\rho = \rho_o \, e^{-\left(\frac{h-h_o}{\alpha_j H_s}\right)} \tag{4}$$

where j = 1 for entry portion of the orbit, and j = 2 for the exit portion. Two different scale height correction factors are used since the spacecraft is within two separate regions of the atmosphere during the entry and exit of the atmosphere. Atmospheric entry occurs approximately between 19° and 11° north latitude, while exit occurs between 11° and 3° north latitude. These correction factors represent changes in the VIRA scale heights that can be related to error in the VIRA model temperature. For example, a correction factor of 1.08 would represent an eight percent deviation from VIRA model temperature. Data analysis using a constant pitch moment coefficient showed that α can be determined to approximately $\pm$ 5%. However, due to the sensitive nature of scale height determination, aerodynamic moment coefficients may not be assumed constant during the aerodynamic event. Rather, a varying moment coefficient must be used as determined by Freemac simulations. Three orbits late in Cycle Four were chosen as test cases for scale height determination. In each of these three orbits, aerodynamic moment coefficients are estimated at twenty second intervals. Figures 3.6, 3.7, and 3.8 show yaw, pitch, and roll aerodynamic moment coefficients, respectively, for orbits #7389, #7503, and #7617. These estimates vary as the result of changing spacecraft attitude relative to the wind velocity vector.

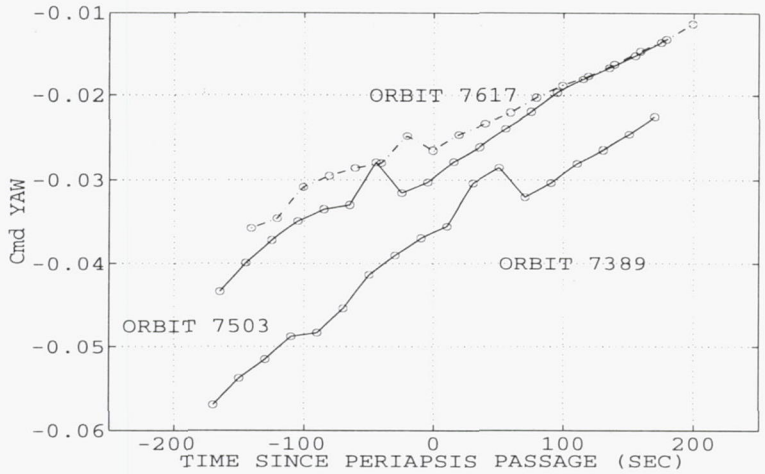

Figure 3.6 Freemac Yaw Aerodynamic Moment Coefficients for Three Orbits

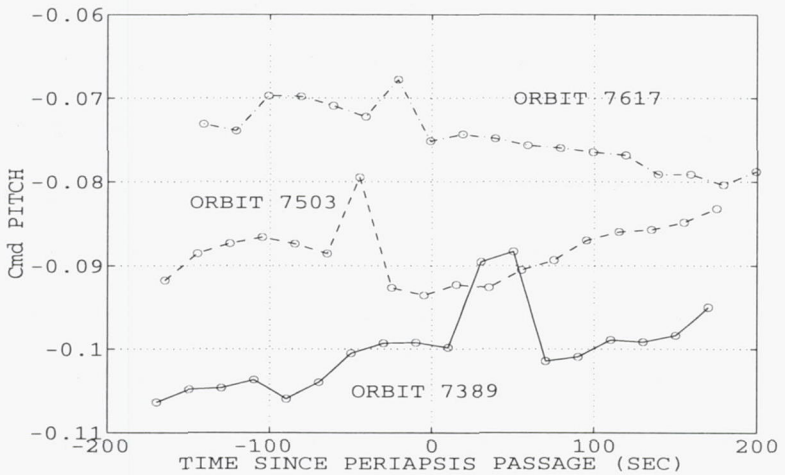

Figure 3.7 Freemac Pitch Aerodynamic Moment Coefficients for Three Orbits

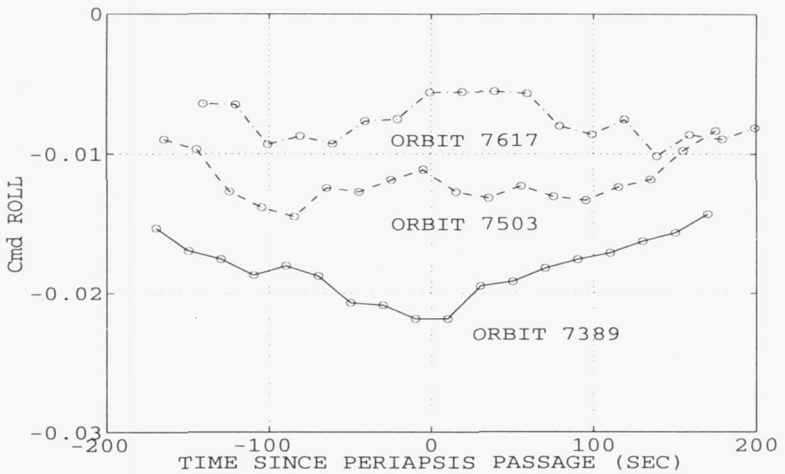

Figure 3.8 Freemac Roll Aerodynamic Moment Coefficients for Three Orbits

Atmospheric parameterization is categorized into two types. In the first case, VIRA scale heights and pitch moment coefficients (Figures 3.4 and 3.5) are assumed correct. Base density and the remaining two aerodynamic moment coefficients are the three parameters estimated. This method of atmospheric analysis will be referred to as the "base density method." For the second approach, five parameters are used. These five parameters are two scale height correction factors, base density, and the yaw and roll aerodynamic moment coefficients. This technique will be called the "scale height method." The scale height method can only be implemented when the pitch moment coefficient is known throughout periapsis passage as shown in Figure 3.7. Also, the spacecraft must experience a large amount of aerodynamic torque in order to successfully measure scale height variation. Such torques are experienced only between orbits #7389 and #7626, therefore, scale height investigation is limited to these orbits. The base density method can be applied to any orbit in Cycle Four.

III.3 Gravity Gradient Torques

Since the gravity field of Venus is not uniform (i.e., gravity follows an inverse-square law), different locations of the spacecraft experience different levels of gravitational attraction toward Venus. The result of this imbalance of forces is a net external torque. It can been shown that a spherical gravity potential is sufficient to accurately model torques due to gravity gradients at Venus. Assuming a spherical potential, torques experienced due to the imbalance of gravitational forces, or gravity gradients, are determined to first order by the equation[13]

$$\vec{T}_g = \frac{3\mu}{R^3}\begin{Bmatrix} \left[mn(I_{zz}-I_{yy})+l(n\,I_{xy}-m\,I_{xz})+(n^2-m^2)I_{yz}\right]\vec{i} \\ +\left[nl(I_{xx}-I_{zz})+m(l\,I_{yz}-n\,I_{xy})+(l^2-n^2)I_{xz}\right]\vec{j} \\ +\left[lm(I_{yy}-I_{xx})+n(m\,I_{xz}-l\,I_{yz})+(m^2-l^2)I_{xy}\right]\vec{k} \end{Bmatrix} \qquad (5)$$

This equation uses moments of inertia and direction cosines to determine gravity gradient torque. The direction cosines, *l*, *m*, and *n*, are defined by the position of Venus in the Magellan spacecraft coordinate system shown in Figure 1.1. The distance between the spacecraft and the planet, R, as well as the gravitational constant, μ, are also known. The only remaining values are the mass moments of inertia, which will be considered unknown. Eq. (5) does not represent a set of independent measurements for the mass moments of inertia. Note that the moments of inertia, I_{xx}, I_{yy}, and I_{zz}, only appear within Eq. (5) as differences. Accordingly, it is not possible to solve for all three moments of inertia, I_{xx}, I_{yy}, and I_{zz}, using the gravity gradient equation. To overcome this problem, I_{xx} was assumed to be known as the calibrated value 1106 kg·m^2. I_{xx} was chosen since it is not affected by solar array orientation. Change in I_{xx} due to propellant mass loss was assumed negligible due to the proximity of the fuel storage tank to the spacecraft yaw axis and the small quantity of fuel used throughout the cycle. Fuel use during Cycle Four caused a change in total spacecraft mass of only 0.04%.

The five parameters to model gravity gradient torque are therefore the five mass moments of inertia: I_{yy}, I_{zz}, I_{xy}, I_{yz}, I_{xz}.

Figure 3.9 represents typical changes in reaction wheel speed due to gravity gradient torques.

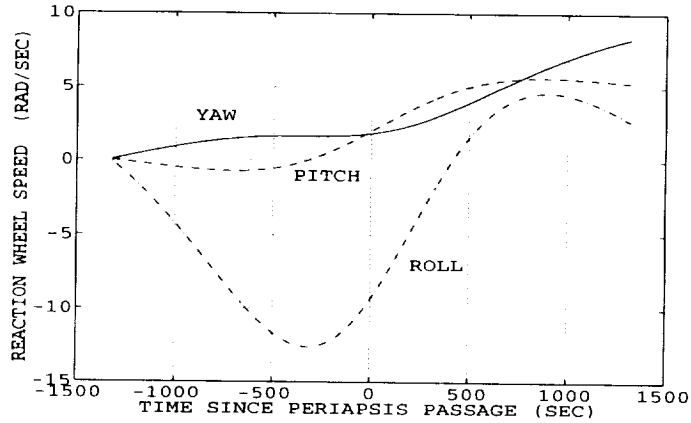

Figure 3.9 Reaction Wheel Speed Due to Gravity Gradient Torque

III.4 Solar Pressure Torques

The final significant contribution to environmental torque is that due to solar pressure. Solar pressure is the result of solar electromagnetic radiation interacting with the spacecraft surface. Similar to the phenomenon associated with atmospheric pressure, there exists some offset between center of solar pressure and spacecraft center of mass. The result is an external torque which is modeled by the equation

$$T_s = -c_{ms}\ p\ A_s\ L_s \tag{6}$$

Eq (6) applies to each of the three body-fixed axes. Mean solar momentum flux is represented by p, while A_s and L_s are respectively, characteristic area (23 m^2) and length (3.66 m). These three values are considered known leaving the solar moment coefficients c_{ms} as the only unknowns. One solar moment coefficient exists for each of the three axes.

As the spacecraft is inertially fixed, any solar moment coefficient is essentially constant over the course of any single orbit. Further, momentum flux does not vary significantly over the periapsis event. Consequently, torque due to solar pressure is constant as long as the sun is visible to the spacecraft. Figure 3.10 shows change in reaction wheel speed due to solar pressure. In this example, there is no change in reaction wheel speed over some time interval near periapsis as the spacecraft passes through the Venus shadow.

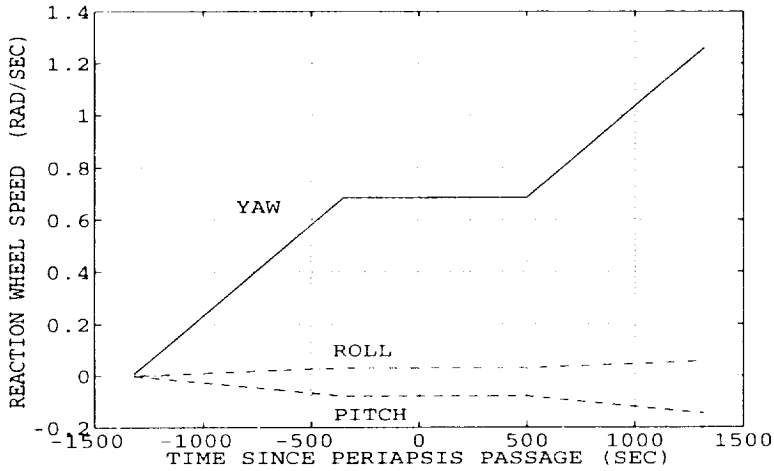

Figure 3.10 Reaction Wheel Speed Due to Solar Pressure Torque

Three parameters are required in order to model solar pressure torque. These parameters are solar moment coefficients corresponding to the yaw, pitch, and roll directions.

III.5 Neglected Torques

Although only atmospheric, gravity gradient, and solar pressure torques are modeled, other environmental torques may exist. Possible causes for these remaining torques are magnetic field interaction and mass discharge. Since Venus does not have an intense magnetic field, magnetic torque is estimated to be on the order of $1 \cdot 10^{-10}$ N·m. This torque is neglected since it is nearly six orders of magnitude less than any of the modeled torques. A mass discharge such as a fuel leak would result in a fairly constant torque. This type of torque would be difficult to notice since it would appear as merely additional solar torque. However, solar occultation could be used to distinguish torque caused by solar pressure from that caused by mass discharge. During occultation, there can be no solar pressure, however, torques caused by mass discharge would continue. Also, mass discharge, such as a fuel leak, would result in an eventually noticeable fuel

loss. Since no significant fuel loss was reported by Martin Marietta during Cycle Four, it is assumed that no torque was caused by mass discharge.

III.6 Final Reaction Wheel Speed Model and Parameters

The total torque model is composed of the individual models described in sections III.2, III.3, and III.4, such that

$$T = T_a + T_g + T_s \tag{7}$$

Eq. (8) through Eq. (11) are used to represent atmospheric, gravity gradient, and solar pressure torques as functions of model parameters. Atmospheric torque is parameterized by two methods. The first, base density method, is given by

$$T_a = T_a(\rho_o, c_{md,yaw}, c_{md,roll}) \tag{8}$$

while the second, scale height method, is

$$T_a = T_a(\rho_o, \alpha_{entry}, \alpha_{exit}, c_{md,yaw}, c_{md,roll}) \tag{9}$$

Gravity gradient parameterization is of the form

$$T_g = T_g(I_{yy}, I_{zz}, I_{xy}, I_{xz}, I_{yz}) \tag{10}$$

and finally, solar pressure is

$$T_s = T_s(c_{ms,yaw}, c_{ms,pitch}, c_{ms,roll}) \tag{11}$$

Reaction wheel speed is then the result of the integration shown in Eq. (1). Three additional parameters are used to represent biases for the yaw, pitch, and roll reaction wheel speeds. A bias parameter represents the speed of a reaction wheel at the beginning of the simulation, and is represented by the constant, C, in Eq. (1). When the base density scheme is used, the model has a maximum of fourteen parameters. On the other hand, the model has at most sixteen parameters for the scale height scheme. Although fourteen or sixteen parameters may be estimated using the above models, it is not always necessary to estimate all parameters. If only base density and aerodynamic moment coefficients are of interest, then solar moment coefficient and the mass moment of inertia parameters may be removed from the model without introduction of significant error.

The following figure shows sample reaction wheel speeds for the pitch direction in order to show relative influence of the atmospheric, gravity gradient, and solar pressure contributions.

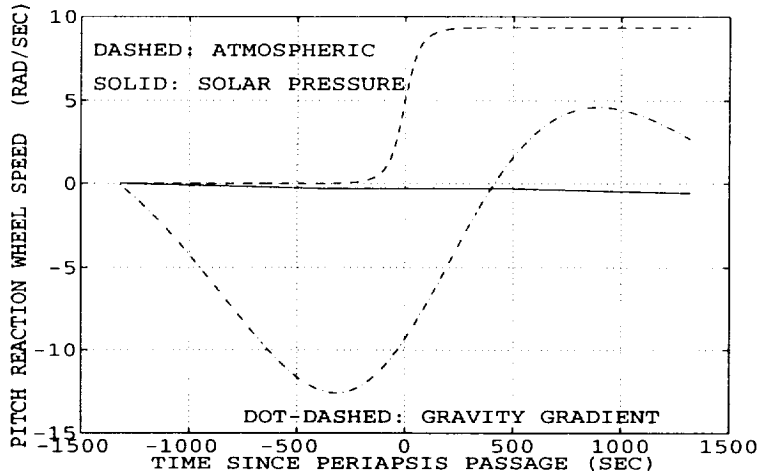

Figure 3.11 Example Contributions to Pitch Reaction Wheel Speed

IV. DIFFERENTIAL CORRECTION

IV.1 Introduction

In order to determine model parameters that best approximate Magellan data, a differential scheme is employed. The general differential correction equations (see Appendix B) are given by

$$\begin{aligned} \Delta\vec{x} &= \left[A_n{}^T \Gamma_\varepsilon^{-1} A_n + \Gamma_x{}^{-1}\right]^{-1}\left[A_n{}^T \Gamma_\varepsilon^{-1}\vec{\varepsilon}_n + \Gamma_x^{-1}(\vec{\mu}_x - \vec{x}_n)\right] \\ \vec{x}_{n+1} &= \vec{x}_n + \Delta\vec{x} \end{aligned} \tag{12}$$

where n is the iteration number, and the sensitivity matrix, A, is given by

$$A_n = \begin{bmatrix} \left.\frac{\partial\omega}{\partial P_1}\right|_{t=1} & \left.\frac{\partial\omega}{\partial P_2}\right|_{t=1} & \cdots & \left.\frac{\partial\omega}{\partial P_M}\right|_{t=1} \\ \left.\frac{\partial\omega}{\partial P_1}\right|_{t=2} & \left.\frac{\partial\omega}{\partial P_2}\right|_{t=2} & \cdots & \left.\frac{\partial\omega}{\partial P_M}\right|_{t=2} \\ \vdots & \vdots & \ddots & \vdots \\ \left.\frac{\partial\omega}{\partial P_1}\right|_{t=N} & \left.\frac{\partial\omega}{\partial P_2}\right|_{t=N} & \cdots & \left.\frac{\partial\omega}{\partial P_M}\right|_{t=N} \end{bmatrix}_n \tag{13}$$

and the measurement and a priori covariance matrices are given respectively by,

$$\Gamma_\varepsilon = \sigma_\varepsilon^2 \begin{bmatrix} 1 & 0 & \cdots & 0 \\ 0 & 1 & \cdots & 0 \\ \vdots & \vdots & \ddots & 0 \\ 0 & 0 & 0 & 1 \end{bmatrix} \qquad \Gamma_x = \begin{bmatrix} \sigma_{x1}^2 & 0 & \cdots & 0 \\ 0 & \sigma_{x2}^2 & \cdots & 0 \\ \vdots & \vdots & \ddots & 0 \\ 0 & 0 & 0 & \sigma_{xM}^2 \end{bmatrix} \tag{14}$$

Once a list of M parameters is specified, Eq. (12) is used to determine the correction to these parameters that minimizes the sum of residuals squared between model and observed data consistent with the a priori information.

IV.2 Parameters

A maximum of sixteen parameters are used to model reaction wheel speed. Parameter selection for reaction wheel modeling is based upon data availability. The following table shows data restrictions for all model parameters.

Reaction Wheel Speed Model Parameter	Reaction Wheel Data Requirement
biases (3)	no restrictions
base density (1)	include ± 400 seconds of periapsis
mass moments of inertia (5)	include ± 15-20 minutes of periapsis
solar moment coefficients (3)	include ± 15-20 minutes of periapsis
aerodynamic moment coefficients (2)	include ± 400 seconds of periapsis
scale height correction factors (2)	include ± 400 seconds of periapsis high rate data strong atmospheric signal

Table 4.1 Data Requirements for Model Parameters

For scale height correction factors, an atmospheric signal is considered strong if it causes a change in reaction wheel speed of 25 rad/sec or more within one orbit. This requires the spacecraft to be below a certain altitude at periapsis depending upon local solar time. Mass moment of inertia and solar moment parameters require data for an extended amount of time due to the low frequency nature of the corresponding torques.

IV.3 A Priori

In Eq. (12), a priori knowledge is represented by the estimate, $\vec{\mu}_x$, and the covariance, Γ_x. The a priori covariance was found to be necessary for convergence only in the case of moment of inertia parameters. Convergence was defined by the iteration when all parameter estimates deviated from the previous iteration's estimates by less than a convergence tolerance. The moment of inertia a priori requirement is attributed to the fact that, depending upon the direction cosines of Eq. (5), some of these parameters are poorly determined on any given orbit. However, in order to prevent the a priori estimates from influencing the actual estimates of moments of inertia, a priori estimates were removed from Eq. (12). This is identical to setting the a priori estimate equal to the value of the current parameter estimate. Thus, the a priori covariance matrix only acts as a conditioning of the information matrix, $A_n^T \Gamma_\varepsilon^{-1} A_n$.[14]

IV.4 Iteration and Convergence

Although the conditioning method assures solution convergence, it dramatically increases the number of iterations required for convergence. As a priori covariance values are lowered, iterations required for convergence increase. Conversely, as a priori covariance values are raised, the possibility of solution divergence increases. Therefore, optimal a priori covariance values exist such that the number of iterations is kept low, but all solutions still converge. These optimal a priori covariance values were found by trial and error and are shown in Table 4.2. No a priori knowledge was used for any parameters other than those representing mass moments of inertia.

Moment of Inertia	A Priori Standard Deviation, σ_x (kg·m²)
I_{yy}	23
I_{zz}	15
I_{xy}	20
I_{xz}	20
I_{yz}	20

Table 4.2 Spacecraft Bus Moments of Inertia A Priori

Unless scale height correction is included in the parameter set, all partial derivatives of Eq. (13) are independent of the model parameters. Iteration is therefore required to minimize the sum of residuals squared only for solutions that include either mass moments of inertia or scale height correction factors.

IV.5 Cramer-Rao Bounds

Cramer Rao bounds are used as formal estimates of accuracy associated with model parameters.[15] The accuracy estimates for all parameters is given by the diagonal values of the inverse of the information matrix, $A_n^T \Gamma_c^{-1} A_n$.

V. RESULTS

V.1 Introduction

The reaction wheel speed model described in section III and the differential correction method outlined in section IV are used to estimate model parameters throughout Cycle Four. The following plot shows a sample orbit simulation where model reaction wheel speed is compared to observed data. The solution set for this example includes three solar parameters, three atmospheric parameters, five moments of inertia,

and three biases. This figure demonstrates the torque model and differential correction's ability to simulate reaction wheel speed.

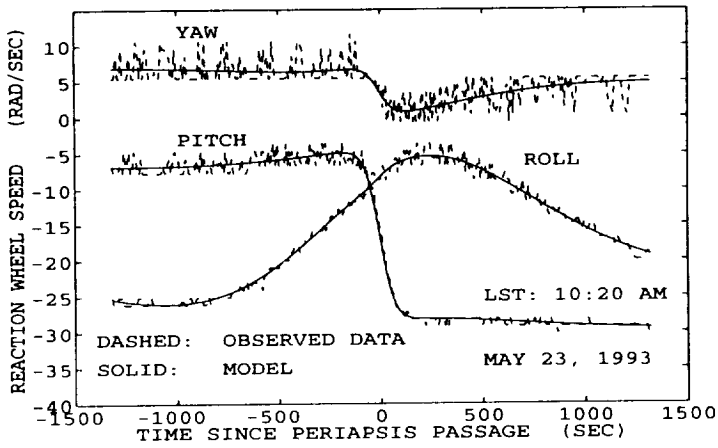

Figure 5.1 Reaction Wheel Speeds for Orbit # 7610

V.2 Atmospheric / Aerodynamic Parameters

The method used to parameterize the torque model for atmospheric and aerodynamic contribution to reaction wheel speed dictates the type of results. Recall that the base density method determines a base density and two aerodynamic moment coefficients. For this method, all solutions are based upon the use of VIRA scale heights. No scale height information is recovered from the base density method, however, it may be applied to all of the orbits of Cycle Four. On the other hand, the scale height method recovers base density, two scale height correction factors, and two moment coefficients. The scale height method requires a strong atmospheric signal which is only present for the final 250 orbits of Cycle Four.

V.2.1 Base Density Method

Base density method is the first method of parameterizing the atmospheric torque contribution of the reaction wheel speed model. Atmospheric torque parameters are base density and two aerodynamic moment coefficients. All results require the use of one previously determined moment coefficient and known VIRA scale heights. The pitch aerodynamic moment coefficients are estimated by free molecular flow simulations. Once this value is assumed known, yaw and roll moment coefficients as well as base density are estimated. The base density method was successfully used on 914 orbits in Cycle Four. Parameters for all orbits were not recoverable for reasons related to limited data coverage. However, for all orbits in which all required information was available, parameter estimates were determined.

V.2.1.1 Base Density

Base density represents atmospheric density at some altitude below spacecraft periapsis altitude. All densities above that altitude are determined from scale heights as shown in Eq. (3). During the time period of this study, spacecraft altitude at periapsis ranges approximately from 165 to 185 km. Base densities are expressed at 165 km for consistency for all of Cycle Four. The following graph compares base densities as found by the reaction wheel method to densities found by the orbital decay technique.[16] The orbital decay method is an independent method of determining base density. For clarity, atmospheric densities determined by orbital decay in Figure 5.2 are multiplied by a factor of ten. This figure shows general agreement of base densities derived from the two independent methods. A dramatic decrease in density occurs during the nighttime. Also, measurements during the nighttime indicate a much larger degree of variability than the daytime.

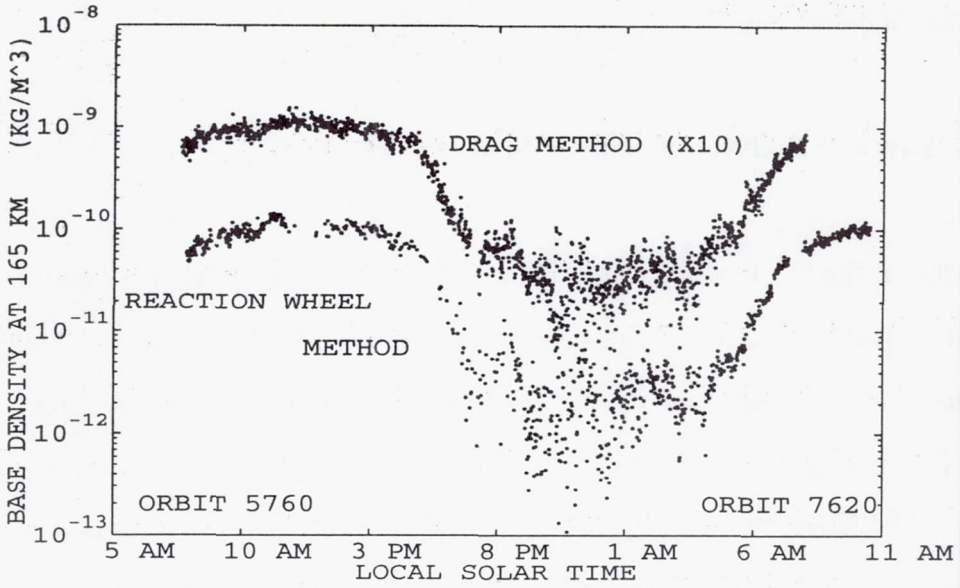

Figure 5.2 Density as Determined By Reaction Wheel Method and Drag Method

When compared on an extended time scale, many of the short term features compare favorably including the "four day period" and nighttime variability. Figure 5.3 shows base densities from Figure 5.2 between 9 AM and 10 AM, early in Cycle Four.

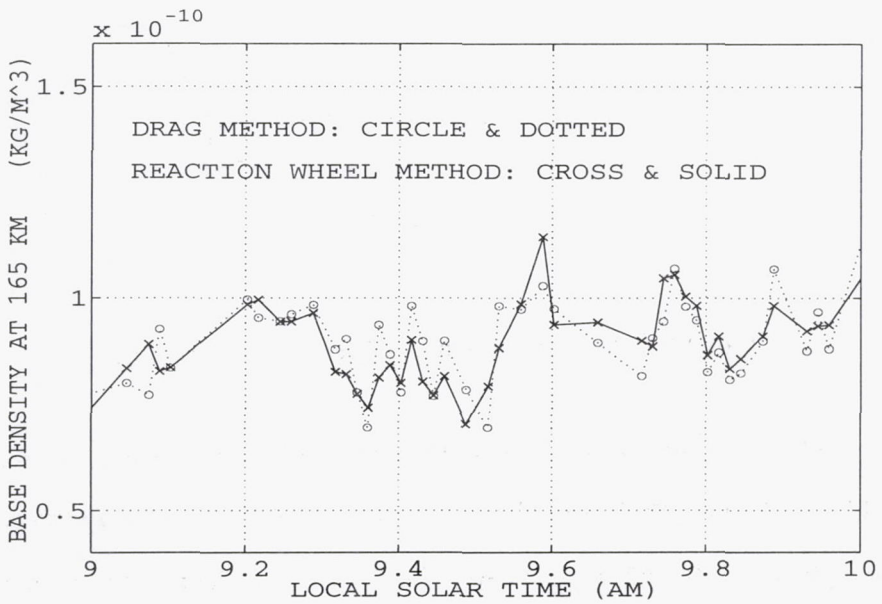

Figure 5.3 Reaction Wheel and Drag Method Base Density Between 9 AM and 10 AM

Figure 5.3 shows agreement between base densities trends as determined by reaction wheel data and drag data.

V.2.1.2 Yaw and Roll Aerodynamic Moment Coefficients

Just as the free molecular flow simulation estimates the pitch aerodynamic moment coefficient, it also estimates the yaw and roll coefficients. These moment coefficients are not used at any time in the base density parameterization method. This provides the opportunity to independently verify consistency between the Freemac moment coefficients. The yaw aerodynamic moment coefficients as estimated by the base density method are shown compared to Freemac values in Figure 5.4.

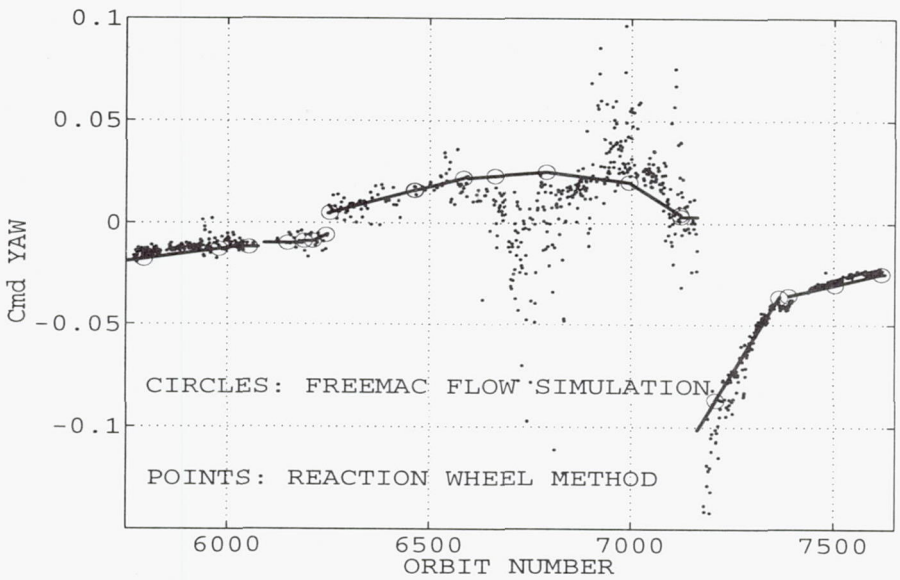

Figure 5.4 Yaw Aerodynamic Moment Coefficient

The yaw moment coefficient shows close agreement between the reaction wheel and the Freemac estimate between orbits #5800 and #6600, as well as between #7250 and #7620. These orbits correspond to daytime local solar hours. During the nighttime, density is considerably lower, making aerodynamic moment measurement more difficult.

The roll aerodynamic moment coefficients as estimated by the base density method is shown compared to Freemac values in Figures 5.5.

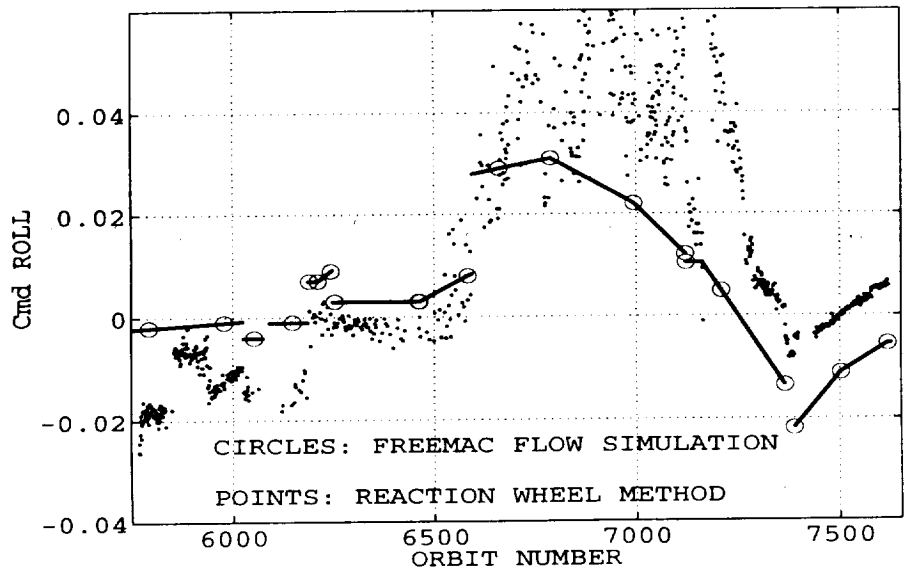

Figure 5.5 Roll Aerodynamic Moment Coefficient

As with the yaw moment coefficient, a large discrepancy appears between orbits #6600 and #7250, for the roll moment coefficient. Again, these orbits occur during the nighttime hours when density is much lower. Also, Freemac estimates of the roll moment are consistently high early in Cycle Four, and are likewise consistently low late in the cycle. This offset could be due to a center of mass located in a different location than assumed by the Freemac model. Current Freemac simulations place the center of mass location on the positive roll axis, 6.259 inches from the yaw-pitch plane. If the offset shown in Figure 5.5 is due to error in spacecraft center of mass location, the sign of this offset indicates that the center of mass is actually above the pitch-roll plane. This is the side of the spacecraft with the altimeter antenna (see Figure 1.1).

Other possible explanations for this disagreement are accommodation coefficients, and solar array position errors within the Freemac model. Momentum and thermal accommodation coefficients are used to characterize the nature the interaction of

an atmospheric particle and the spacecraft surface. The coefficients dictate the amount of energy and momentum absorbed by the spacecraft. Errors in these coefficients may cause significant error in aerodynamic moment coefficients. Errors in positions of the solar arrays may also affect aerodynamic moment coefficients. Solar array position has an uncertainty of $\pm$ 0.5 degrees under nominal conditions, however, this error may increase dramatically during occultation. During this time, sun-sensors are unable to track the sun and solar array position error may increase to 11°. This error is caused by non-linear effects of solar array position potentiometers (Personal communication, M. Patterson, Martin Marietta Corporation, March 10, 1994). This error should only appear during occultation which corresponds approximately to orbits #6600 through #7200. This type of solar array position error can therefore not be responsible for the roll offset shown in Figure 5.5 during late and early Cycle Four.

V.2.2 Scale Height Method

The second method of parameterizing the atmospheric torque model allows the examination of scale heights in addition to base density. In this case, the method estimates a base density, two scale height correction factors, and the yaw and roll aerodynamic moment coefficients. The base density again represents density at some base altitude below the altitude of spacecraft periapsis. Densities above that altitude are determined from Eq. (4). Scale height correction factors, α, are used to modify VIRA scale heights. Whereas the base density method needs only one constant pitch moment value from Freemac, the scale height method requires that pitch moment coefficients be known throughout the orbit. The yaw and roll moment coefficients are estimated as single, constant values for a given orbit. If the Freemac yaw and roll moment coefficients are consistent with the pitch coefficient, it would be expected that the scale height method estimates should be approximate averages of the Freemac estimates.

Base densities recovered using the scale height method will vary slightly from the solutions from the base density method. However, these solutions only vary due to the change in scale heights. Accordingly, base density estimates recovered using this method are not shown.

V.2.2.1 Scale Heights

Two scale height correction factors are determined for each orbit. The first represents deviation from VIRA scale heights within the atmospheric entry portion of the orbit (in), while the second represents the exit of the atmosphere (out). The entry portion of the orbit corresponds approximately to a region from 19° to 11° north latitude. Similarly, the exit portion occurs from 11° to 3° north latitude. Scale height correction factors are used to calculate modified scale heights.

Figures 5.6 and 5.7 demonstrate the ability of reaction wheel data to recover information related to spatial variation in atmospheric density. This graph represents example residuals before and after applying the scale height correction factors. A spline filter is used to smooth residuals for purposes of presentation. When VIRA scale heights are used rather than modified scale heights, the differential correction algorithm is unable to fit the observed data to the noise level, i.e., some type of signal appears within the residuals. This signal is shown by the dashed lines of Figures 5.6 and 5.7. However, scale heights can be modified such that this signal is removed from the residuals. Scale heights are modified by multiplying each scale height by the appropriate scale height correction parameter, α. In these two figures, solid lines represent residuals after using modified scale heights. Essentially all signal is thus removed from the residuals and scale height information is recovered.

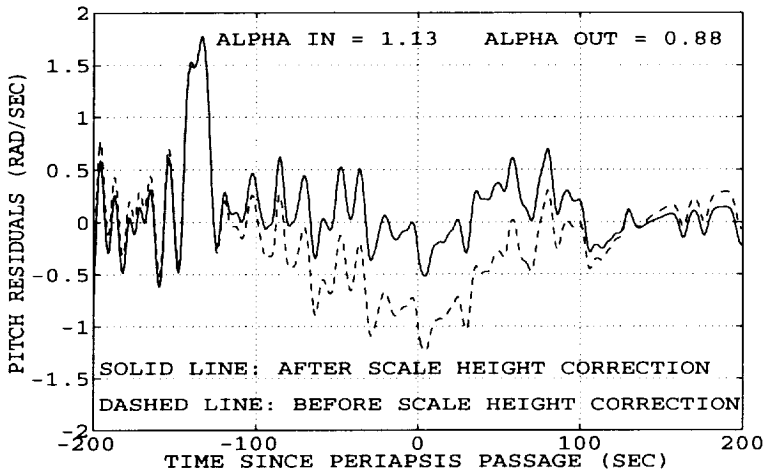

Figure 5.6 Scale Height Correction Effect on Residuals of Orbit #7511

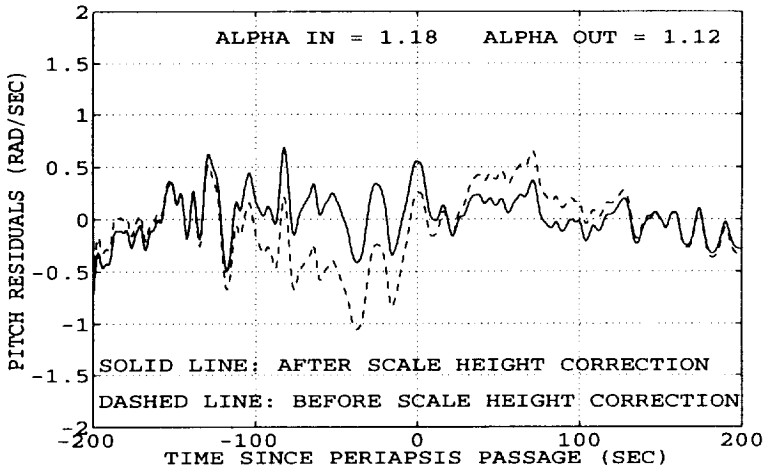

Figure 5.7 Scale Height Correction Effect on Residuals of Orbit #7479

Scale height determination was completed for approximately 150 orbits late in Cycle Four. As stated above, scale height determination requires Freemac estimates of the pitch moment coefficient as it varies through the orbit. These pitch moment coefficients, shown in Figures 3.6, 3.7, and 3.8, are available for orbits #7389, #7503, and #7617. For orbits that the aerodynamic coefficients are not available, the nearest orbit's estimates are used. These coefficients are estimated at twenty second intervals throughout the atmospheric event. A linear interpolation is used to determine pitch moment coefficients at times within these twenty second intervals.

Figure 5.8 shows recovered scale heights for the atmospheric entry portion of the orbit. Likewise, Figure 5.9 shows scale heights for the exit portion of the orbit. These values are plotted in comparison to VIRA scale heights. The VIRA model is primarily based on Pioneer-Venus drag data which represented the atmosphere at 11° south latitude. The VIRA model does not include any latitudinal variation and therefore does not make a distinction between the entry and exit scale heights. Recovered scale heights are filtered using a spline method to show general trends. These figures indicate a large degree of variability. Sample standard deviations of these measurements correspond to a variation of approximately ±7% of respective mean scale heights. If attributed only to changes to atmospheric temperature, this variation suggests changes of ±20° C within the 3.25 hour period of Magellan orbit, however, it is important to note that some of the variation seen in Figures 5.8 and 5.9 may be the result of measurement uncertainty.

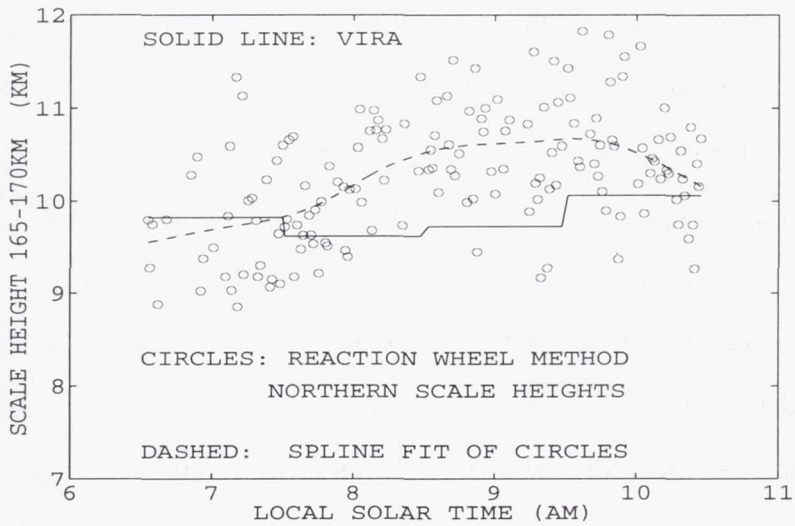

Figure 5.8 VIRA and Recovered Scale Heights (19° to 11° North Latitude)

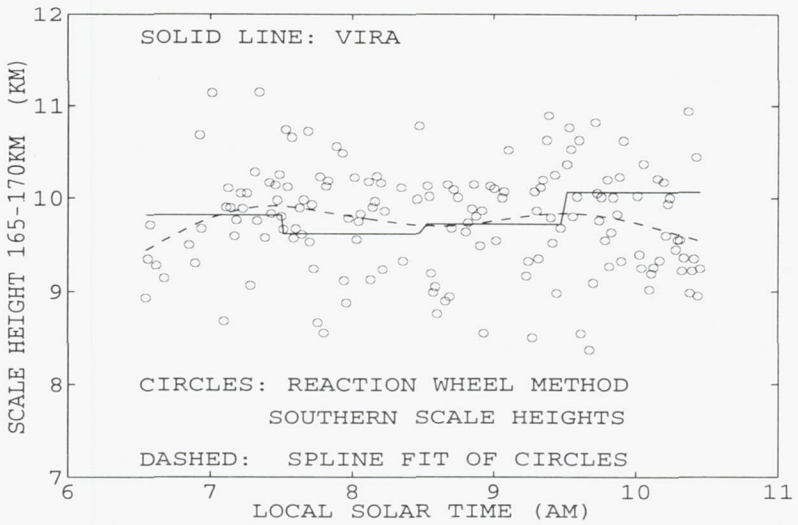

Figure 5.9 VIRA and Recovered Scale Heights (11° to 3° North Latitude)

Figures 5.8 and 5.9 indicate that scale heights are higher in the northern than the southern latitudes. This suggests that atmospheric temperatures are higher from 19° to 11° north latitude than from 11° to 3°, contradicting current theories of temperature variation in the Venusian atmosphere. The most likely cause for an error in scale height measurement is the Freemac pitch aerodynamic moment coefficient. A brief study confirmed that erroneous aerodynamic moment coefficients can cause large scale height errors. Figure 5.9 shows scale heights that are consistent with VIRA scale heights, while Figure 5.8 shows scale heights that are higher that VIRA after 8 AM LST. Transient accommodation coefficients may account for these higher scale height indications in the northern latitudes. Current Freemac aerodynamic simulations assume a constant accommodation coefficient for the entire atmospheric event. If the accommodation coefficient, and accordingly the pitch moment coefficient, were changing during the atmospheric event, scale height measurements would be in error.

Another important consideration for scale height measurement is sensitivity to time of periapsis. Error in time of periapsis may result from either poor orbit determination or inaccuracy of the spacecraft clock. Either type of time error would

result in an atmospheric torque anomaly similar to that of scale height error. For this reason, scale height measurements are now examined as a function of time of periapsis error.

Figure 5.10 shows scale height correction factor, as error is introduced to time of periapsis.

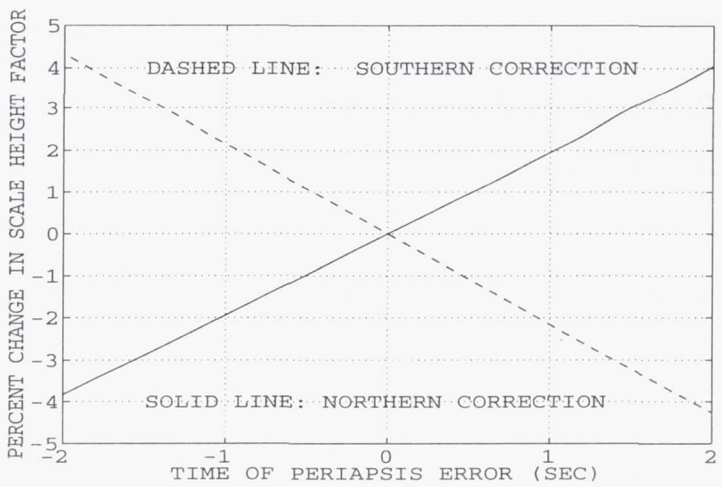

Figure 5.10 Scale Height Correction Factor Sensitivity to Time of Periapsis Error

The first is uncertainty associated with the spacecraft clock, however, this error is small since the onboard clock is calibrated to 8 milliseconds of Universal Time.[17] Error may also be introduced by the orbit determination. Time of periapsis as determined by Doppler data is considered to be known better than 0.1 seconds for the Magellan orbit late in Cycle Four (Personal communication, Kuen Wong, Jet Propulsion Laboratory, March 29, 1994). Figure 5.10 indicates that this error is acceptable for scale height measurements.

V.2.2.2 Yaw and Roll Aerodynamic Moment Coefficients

Yaw and roll aerodynamic moment coefficients are also determined by the scale height method. Although Freemac estimates moment coefficients for attitudes near periapsis, this reaction wheel method only estimates two constant coefficients, i.e., one coefficient for each direction. These two estimates represent the average aerodynamic yaw and roll moment coefficients during the atmospheric event. As in the case of the base density method, the yaw and roll moment coefficient can be compared with Freemac estimates to evaluate consistency. Figure 5.11 shows yaw moment coefficient as determined by Freemac compared to the estimate by the scale height method. The reaction wheel derived estimate appears to be close to the average value of the Freemac estimate, therefore confirming consistency between the yaw and pitch moment coefficient.

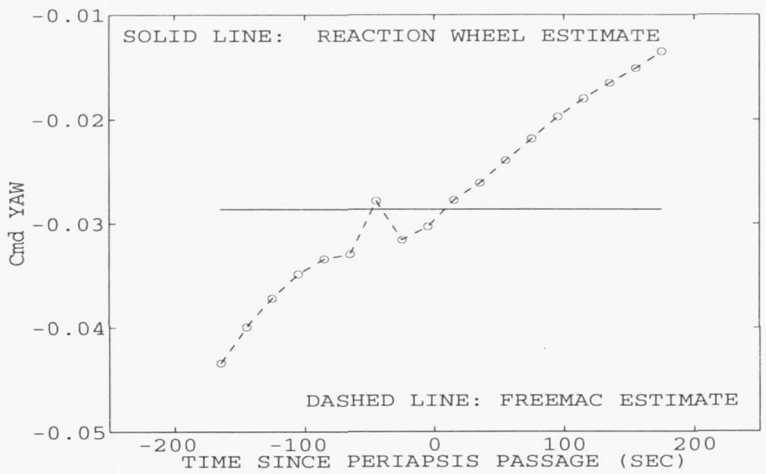

Figure 5.11 Yaw Aerodynamic Moment Coefficient for Orbit #7503

Likewise, the roll aerodynamic coefficient as estimated by reaction wheel data is compared to the Freemac estimate in Figure 5.12. This figure shows the same type of inconsistency that was indicated by the base density method shown in Figure 5.5.

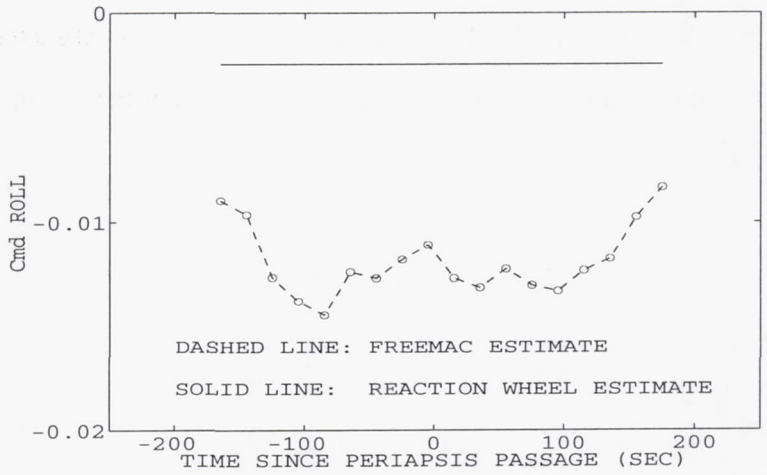

Figure 5.12 Roll Aerodynamic Moment Coefficient for Obit #7503

V.3 Mass Moments of Inertia

Since I_{xx} was assumed to be known in all solutions, only five moments of inertia were determined. Changes in moments of inertia during Cycle Four can be attributed to movement of the solar arrays. By knowing solar array position and mass distribution (Personal communication, H. Curtis, Martin Marietta Corporation, June 4, 1993) of the solar arrays, a theoretical model of moment of inertia variation was developed (see Appendix C). The solar arrays were modeled as thin plates of mass 35 kg, based on preflight properties. This solar array model contributes to total spacecraft moments through $I_{xx} = 37\ kg{\cdot}m^2$, $I_{xy} = I_{xz} = 0$. The remaining moments of inertia are functions of the solar array position. Total moments of inertia, as used by Eq. (5), can then be determined as the sum of moments of inertia of the Magellan spacecraft bus and the solar arrays. The differential correction algorithm was designed to estimate values of spacecraft bus moments of inertia. Figures 5.13 through 5.20 show modeled moments of inertia of the solar arrays and estimates of the spacecraft bus moments of inertia. Discontinuities appear in the solar array moment of inertia curves due to solar array off point adjustments. Moments of inertia are not determined between orbit #5938 and orbit

#6462 due to limited data coverage. Figures of solar array model moments of inertia are headed by the model equation as derived in Appendix C. Figures of estimated bus moments of inertia also contain error bars indicating measurement mean and standard deviation.

$$I_{yy} = 813 + 37\cos^2\beta \quad (kg \cdot m^2)$$

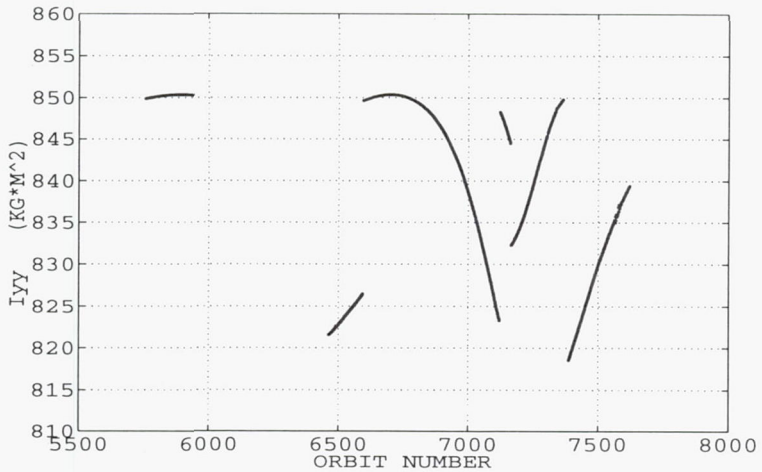

Figure 5.13 Model Mass Moment of Inertia I_{yy} of Magellan Solar Arrays

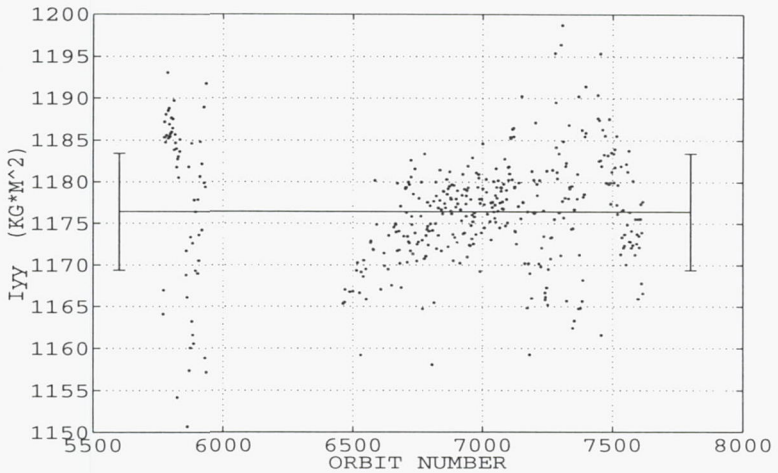

Figure 5.14 Estimated Mass Moment of Inertia I_{yy} of Spacecraft Bus

As shown in Table 4.2, the a priori standard deviation used for I_{yy} is 23 kg·m^2. All estimates of I_{yy} clearly lie within ± 23 kg·m^2 of the estimated mean. Therefore, estimates are considered not to be restricted by the a priori covariance. Some correlation exists between the solar array model and spacecraft bus estimates of I_{yy}, probably due to a slight error in the solar array model.

$$I_{zz} = 813 + 37\sin^2\beta \quad (kg \cdot m^2)$$

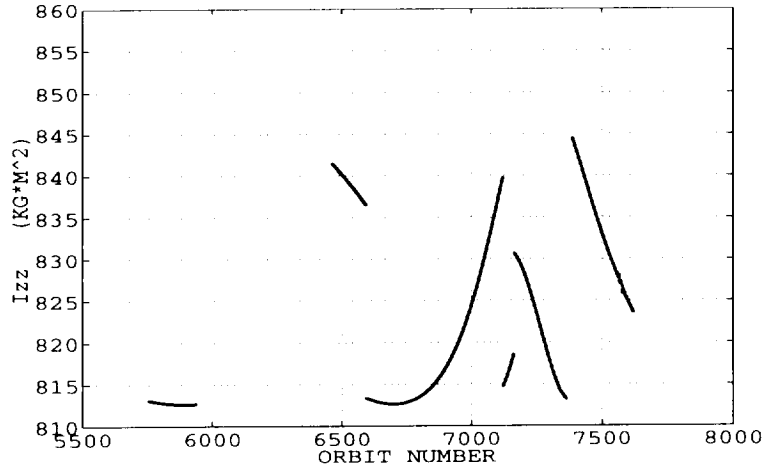

Figure 5.15 Model Mass Moment of Inertia I_{zz} of Magellan Solar Arrays

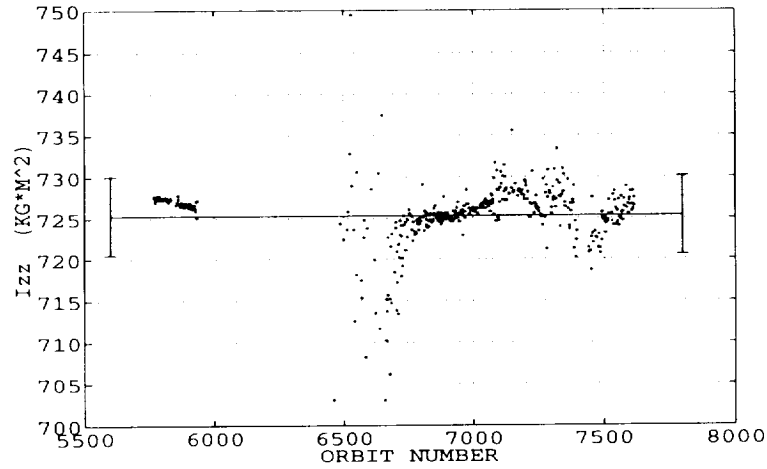

Figure 5.16 Estimated Mass Moment of Inertia I_{zz} of Spacecraft Bus

For the estimate of spacecraft bus I_{zz}, Table 4.2 indicates an a priori standard deviation of 15 kg·m^2. Figure 5.16 shows this parameter not to be restricted by the a priori covariance. A positive correlation exits between the solar array and bus I_{zz} values before the conjunction roll maneuver (orbit #7164) and a negative correlation exits afterwards. This again suggests a small error in the solar array moment of inertia model.

$$I_{yz} = 19\sin 2\beta \quad (kg \cdot m^2)$$

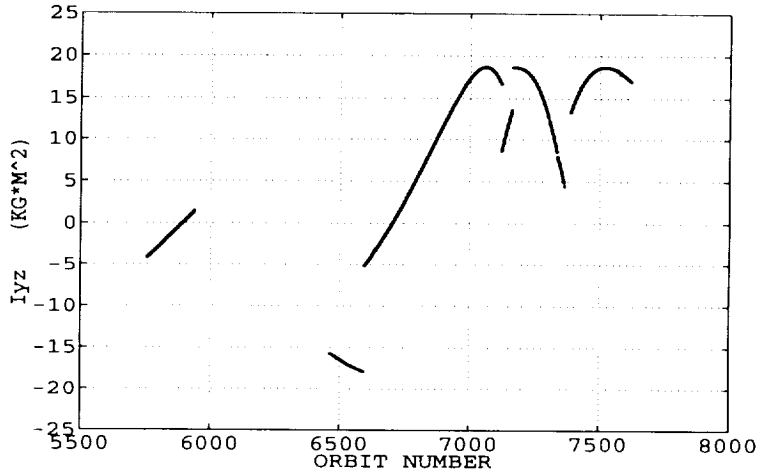

Figure 5.17 Model Mass Product of Inertia I_{yz} of Magellan Solar Arrays

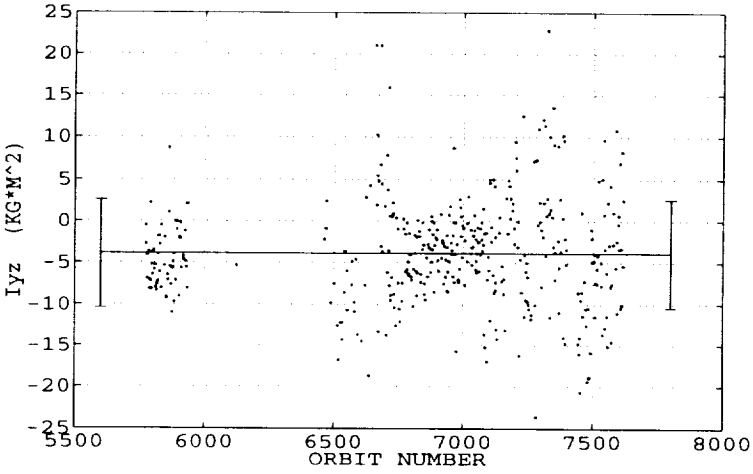

Figure 5.18 Estimated Mass Product of Inertia I_{yz} of Spacecraft Bus

A priori standard deviation for I_{yz} is 20 kg·m^2. Estimates are not restricted by this a priori information. No correlation is apparent between the estimated spacecraft bus and modeled solar array I_{yz}.

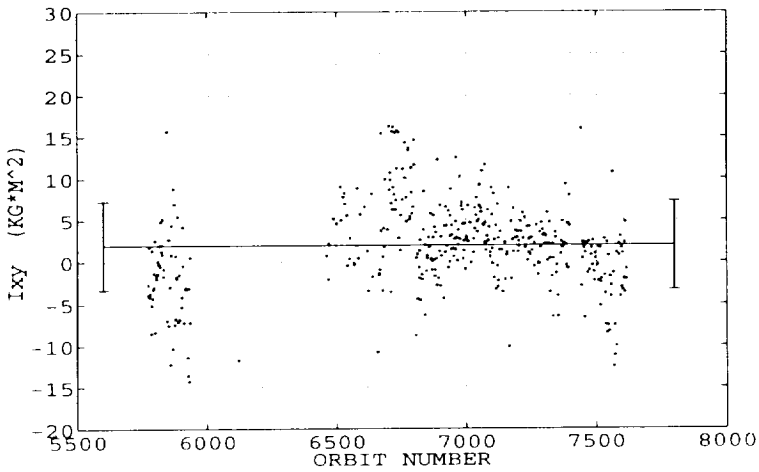

Figure 5.19 Estimated Mass Product of Inertia I_{xy} of Spacecraft Bus

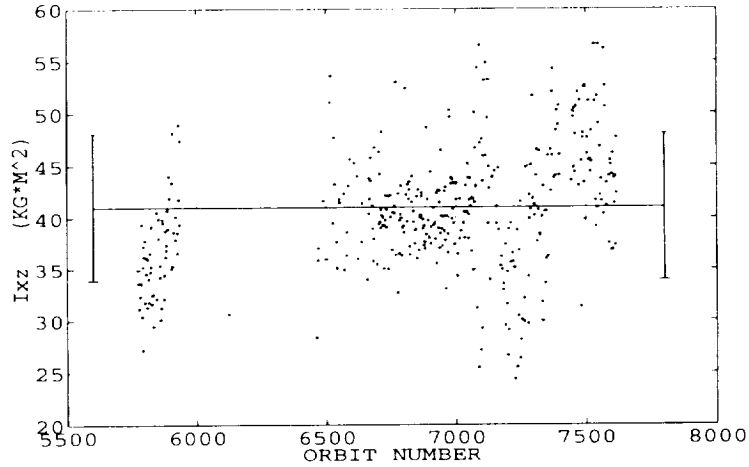

Figure 5.20 Estimated Mass Product of Inertia I_{xz} of Spacecraft Bus

Modeled solar array moments of inertia I_{xy} and I_{xz} are not shown since they are identically zero. A priori standard deviations for I_{xy} and I_{xz} are both 20 kg·m^2. Figures

5.19 and 5.20 show these estimates are not restricted by the a priori. These two figures also show no significant trends indicating solar array moment of inertia correlation.

Mean values and standard deviations of the estimated moments of inertia from Figures 5.14, 5.16, 5.18, 5.19, and 5.20, are shown in Table 5.1.

Moment/Product of Inertia	Mean ($kg \cdot m^2$)	Standard Deviation ($kg \cdot m^2$)
I_{yy}	1176.4	7.0
I_{zz}	725.3	4.8
I_{xy}	2.0	5.3
I_{xz}	41.0	7.1
I_{yz}	-3.9	6.5

Table 5.1 Spacecraft Bus Mean Estimated Moments of Inertia

Total moments of inertia were determined by adding bus and solar array moments of inertia. Maximum and minimum values occur when the solar arrays pass through either the spacecraft XY or XZ plane as shown in Table 5.2. I_{xx} is highlighted to indicate that it is not an estimated parameter. Mass moment of inertia values as estimated by an in-flight calibration performed by Martin Marietta are also included in Table 5.2.

Moment/Product of Inertia	Solar Array in XY Plane ($kg \cdot m^2$) *Reaction Wheel Method Estimate*	Solar Array in XY Plane ($kg \cdot m^2$) *Martin Marietta Calibration*	Solar Array in XZ Plane ($kg \cdot m^2$) *Reaction Wheel Method Estimate*
I_{xx}	1106	1106	1106
I_{yy}	1989.1	1975	2026.4
I_{zz}	1575.3	1577	1538.0
I_{xy}	2.0	2.55	2.0
I_{xz}	41.0	37.4	41.0
I_{yz}	-3.9	1.1	-3.9

Table 5.2 Magellan Spacecraft Total Moments of Inertia

V.4 Solar Pressure Moment Coefficients

Solar parameters were determined for Cycle Four in the form of c_{ms}. These parameters were not determined before orbit #6462 due to limited data coverage. One such parameter exists for each coordinate axis; yaw, pitch, and roll. Solar moment coefficients are plotted as a function of solar longitude. This Solar longitude is defined within the spacecraft coordinate system as the angle between the roll axis and the sun-vector projected into the pitch-roll plane. Solar latitude is then defined by the elevation of the sun-vector above the pitch-roll plane. Figure 5.21 shows the solar longitude and latitude definition

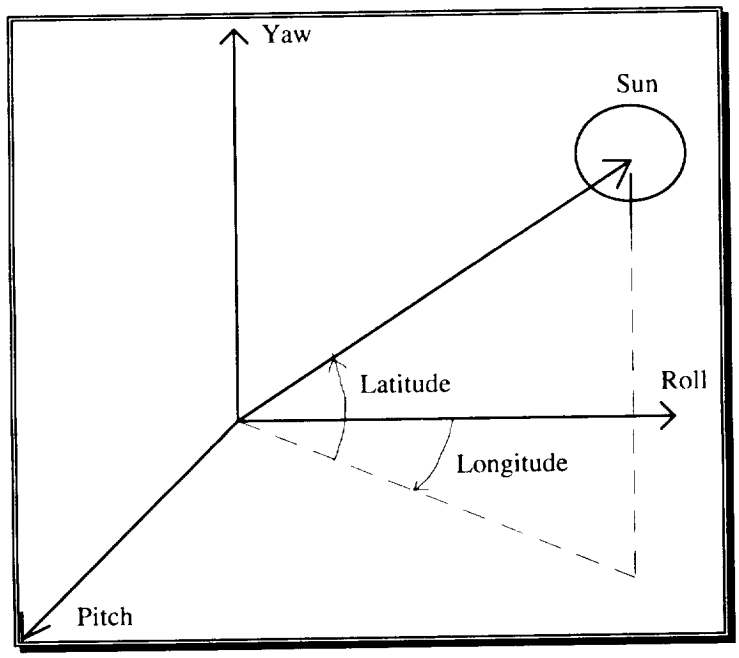

Figure 5.21 Solar Longitude and Latitude Definition

Figure 5.22 shows solar longitude and latitude for Cycle Four. The solar latitude is near -10° for much of Cycle Four due to the 10° Earth-point roll (see Appendix E, Figure E.15).

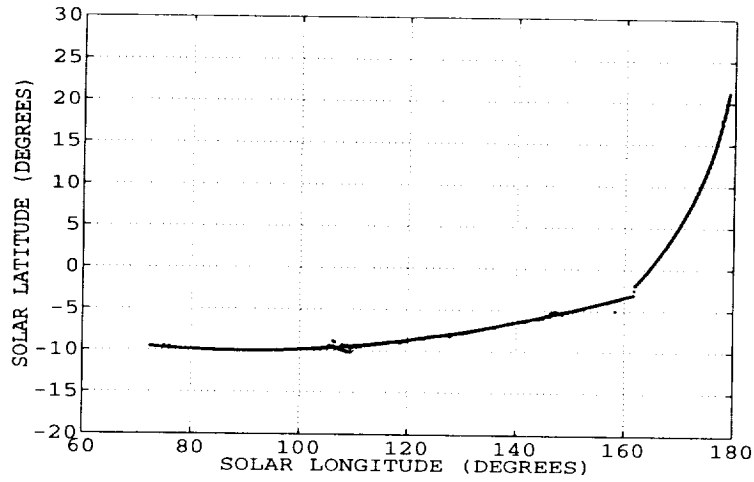

Figure 5.22 Cycle Four Solar Longitude and Latitude

Since the spacecraft rolls 180° prior to conjunction, solar longitude never increases above 180°. Thus, the same side of the spacecraft always faces the sun. Solar longitude starts at approximately 70° and proceeds toward 180° as the sun appears to rotate about the spacecraft. After conjunction and completion of the spacecraft roll maneuver, the solar longitude returns toward 70°. Large values of solar latitude near conjunction result from the rolling spacecraft.

Figures 5.23, 5.24, 5.25, show c_{ms} for Cycle Four. In these figures, circles represent orbits prior to conjunction and crosses represent orbits after conjunction.

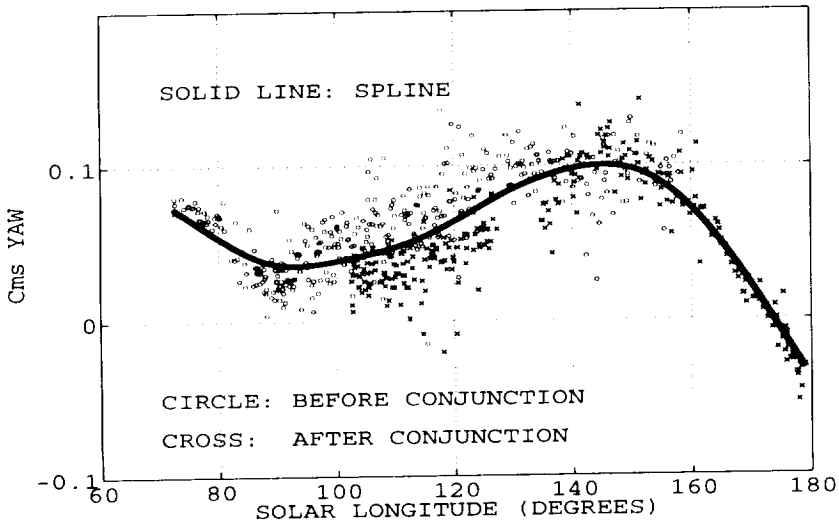

Figure 5.23 Estimated Yaw Solar Moment Coefficient for Cycle Four

The yaw solar moment coefficient shows a clear minimum when solar longitude is 90°. It also approaches zero as solar longitude approaches 180°. The maximum yaw moment coefficient corresponds to a solar longitude of 145°. Solar torque in the yaw direction is largely the result of the High Gain Antenna (HGA). At 90° the cross sectional area presented to the sun by the HGA is a minimum, thus causing the minimum moment coefficient. At 180° the HGA shows a large cross section for solar pressure, but the net force acts through the yaw axis, thus causing no torque. A maximum occurs somewhere between 90° and 180° where the HGA causes the largest product of cross sectional area and moment arm. This corresponds to 145° according to Figure 5.22. The symmetric nature of the spacecraft should cause the yaw moment coefficient to be symmetric about the solar longitude angle 90°, such that another maximum would occur at 35° solar longitude and another zero at 0° solar longitude.

Estimates of the yaw moment coefficient appear to have slightly different values before and after conjunction, but still follow the same trends.

Figure 5.23 shows a yaw moment coefficient that is not exactly zero at a solar longitude of 180°. This is most likely explained by "shadowing" effects of the solar arrays caused by the high solar latitude shown in Figure 5.22.

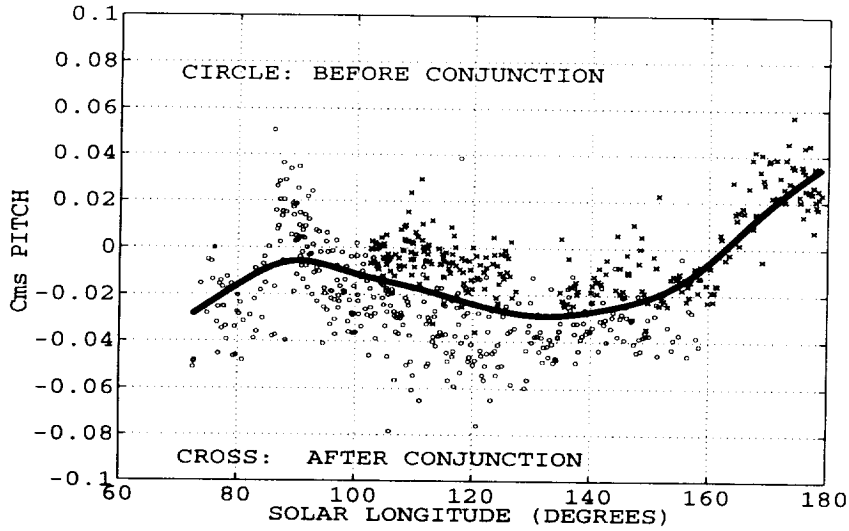

Figure 5.24 Estimated Pitch Solar Moment Coefficient for Cycle Four

Figure 5.24 indicates that the largest torque in the pitch direction due to solar pressure occurs when the solar longitude is between 170° and 180°. At this time, solar latitude reaches its maximum value of 20°, as shown in Figure 5.20. This high solar latitude is responsible for the high solar pitch moment coefficient. As expected, a zero in the pitch coefficient occurs near a solar longitude of 160° when the latitude is also zero. The pitch moment coefficient also approaches zero as solar longitude nears 90°. This is the result of the net solar pressure force acting almost completely in the pitch direction. Under this condition, little torque can be created about the pitch axis.

Figure 5.25 shows the roll solar moment coefficient. This figure indicates that the roll direction experiences very little torque due to solar pressure.

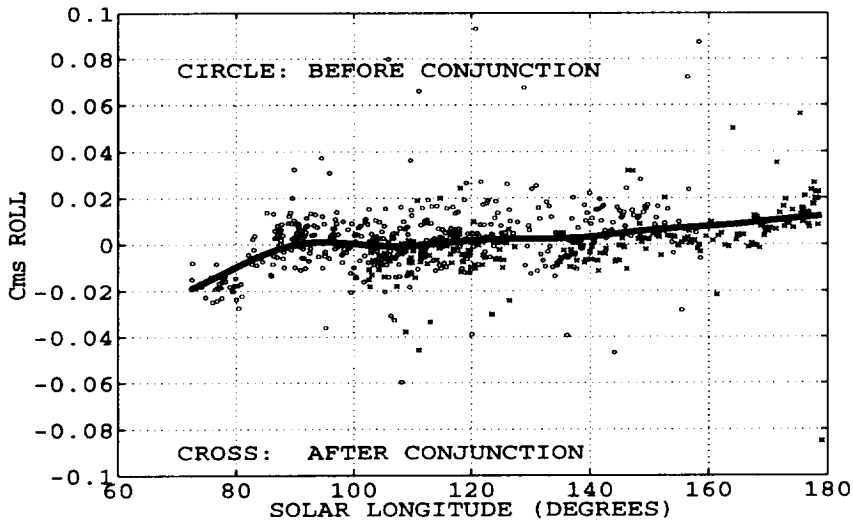

Figure 5.25 Estimated Roll Solar Moment Coefficient for Cycle Four

VI. ACCURACY ANALYSIS

VI.1 Introduction

An accuracy estimate for a given parameter is obtained directly from the information matrix, $A_n^T \Gamma_\varepsilon^{-1} A_n$. Namely, Cramer-Rao bounds are used as indicators of the accuracy of estimated parameters. The measurement covariance matrix, Γ_ε, is given by Eq. (14), where $\sigma_\varepsilon^2 = 0.0827\ rad^2 / \sec^2$. This value is derived from estimating the standard deviation of a uniform distribution of values within the quantization error of the reaction wheel tachometer. The definition of the measurement covariance matrix in Eq. (14) assumes no correlation between successive data points. Such a correlation would result in values for the off-diagonal terms of this matrix.

Accuracy estimates are also recovered by examining the statistics of estimates of parameters that do not have a large degree of natural variability. Parameters such as moment coefficients and mass moments of inertia should not vary significantly from orbit

to orbit. Standard deviations of these estimates thus provide a valid estimate of a parameter's measurement "repeatability."

Determining the accuracy associated with mass moment of inertia parameters using Cramer-Rao bounds, is complicated by the a priori requirements. For solutions containing these parameters, conditioning the information matrix with a priori covariance is necessary in order to determine the inverse. For this reason, accuracy of moment of inertia parameters is estimated by statistical analysis of the final estimates only.

VI.2 Base Densities

Accuracy estimates for the base density and scale height method are essentially the same. For this reason, error analysis is presented only for the base density method since it represents the entirety of Cycle Four. Figure 6.1 shows normalized accuracy for base density. In this case, the accuracy estimate is normalized by dividing by the base density for the given orbit. Crosses are used to indicate orbits where high rate data was available, while circles represent the low rate.

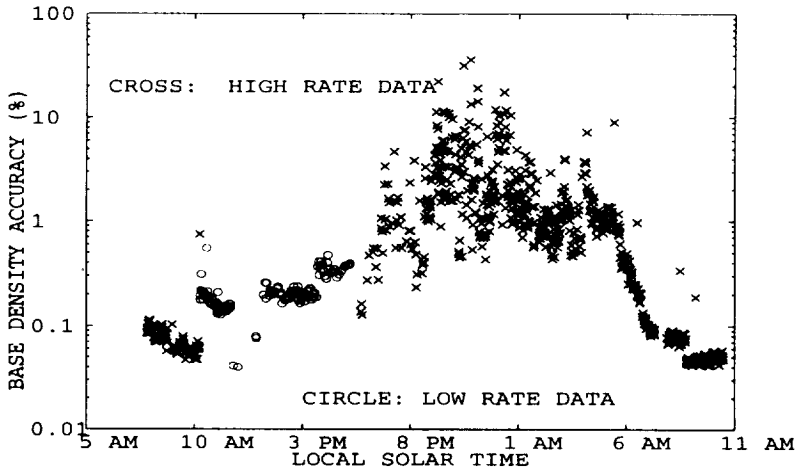

Figure 6.1 Normalized Base Density Accuracy Estimate

Accuracy decreases dramatically during nighttime local solar times. During this period, atmospheric base density is much lower than during the daytime. Accordingly, the signal-to-noise ratio is significantly lowered, resulting in lower normalized accuracy. During the daytime, accuracy are generally better than 0.5%. This is of course more accurate than the pitch aerodynamic moment coefficient estimate by Freemac, therefore, the limiting factor in determining base density from reaction wheel data is the pitch moment coefficient. Near a local solar time of 10 AM, transmitted data went from the high to the low rate. A noticeable decrease in accuracy occurs at this time, indicating the method's sensitivity to data transmission rate. Cramer-Rao bounds indicate a measurability threshold for density of $8 \cdot 10^{-13}$ kg/m^3 for high rate data and $4 \cdot 10^{-12}$ kg/m^3 for low rate data.

VI.3 Yaw and Roll Aerodynamic Moment Coefficients

Accuracy estimates for the yaw and roll moment coefficients are presented in a different fashion than the base density. Aerodynamic moment coefficients may have values very close to zero, making the normalized accuracy undefined. For this reason, absolute accuracy estimates are shown for the yaw and roll moment coefficient as determined by Cramer-Rao bounds. Figure 6.2 shows these values for the yaw moment coefficient. Again, crosses indicate high rate and circles represent low rate data.

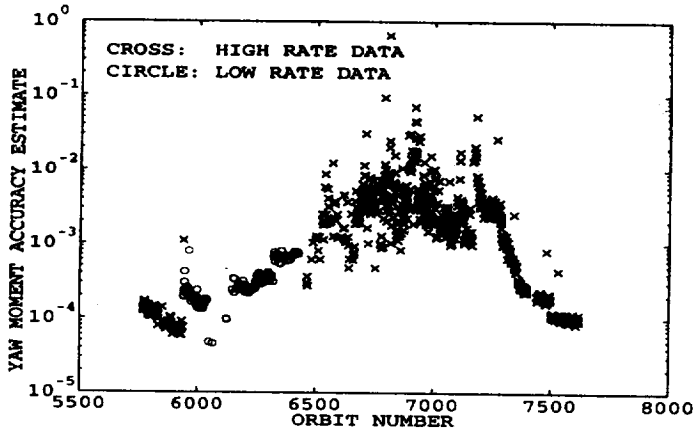

Figure 6.2 Yaw Aerodynamic Moment Coefficient Accuracy Estimate

Again, accuracy decreases significantly after sunset, and then increases after sunrise. After sunset, base densities drop making aerodynamic measurement more difficult. The lower transmission rate also decreases the yaw moment coefficient accuracy. Cramer-Rao bounds indicate a measurement threshold of 0.001 during the daytime.

Figure 6.3 shows the roll moment coefficient accuracy estimate.

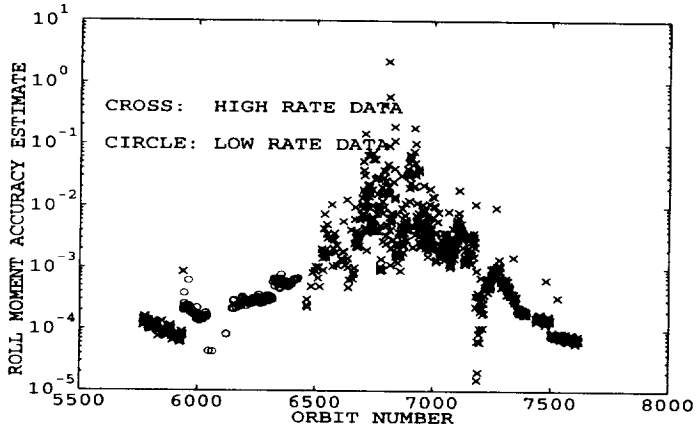

Figure 6.3 Roll Aerodynamic Moment Coefficient Accuracy Estimate

Figure 6.3 repeats the same trends as base density and the yaw moment coefficient for local solar times and transmission rates. Measurement threshold for the roll aerodynamic

moment coefficient, as determined by Cramer-Rao bounds, is essentially the same as the yaw moment coefficient.

In order to validate the Cramer-Rao error estimates for the yaw and roll aerodynamic moment coefficients, the "scatter" of the actual measurements as shown in Figures 5.4 and 5.5 is examined. Breaking the estimates into 38 groups of 24 orbits allows for statistical analysis of the measurement. Each group of 24 orbits is used to determine one sample mean and standard deviation. Figure 6.4 shows these sample standard deviations.

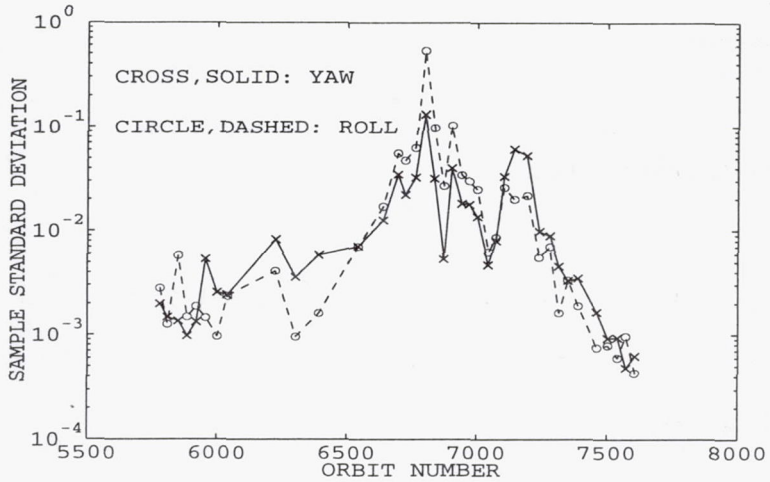

Figure 6.4 Yaw and Roll Aerodynamic Moment Coefficient Sample Standard Deviation

Figure 6.4 indicates a factor of ten lower sample accuracy during the daytime than Figures 6.2 and 6.3. This disagreement indicates that the current error model is not correct. One of the primary assumptions of the error model is that the data is a uniform distribution within the measurement quantization. Close examination of the observed reaction wheel speed as received from the telemetry stream reveals that the signal is not always contained within the measurement quantization as explained in section II.3. As reaction wheel speed approaches zero, the measurements noise increases to as much as ±

2.5 rad/sec. A uniform distribution of ±2.5 produces a measurement covariance of $\sigma_\varepsilon^2 = 2.08\ rad^2 / \sec^2$. This is approximately 25 times larger than the covariance when the data is assumed to stay within the measurement quantization. Estimated error from Cramer-Rao bounds would have been five times larger if this large covariance was used. As the reaction wheel increases speed, the measurements tend to return to within ± 0.5 rad/sec, but not until the reaction wheel achieves a speed of nearly 25 rad/sec. This variation can be seen in the observed reaction wheel speed signal of Figure 5.1. The measurement standard deviation is therefore a function of reaction wheel speed. A more sophisticated error model would take into account this variation in standard deviation of reaction wheel measurements.

VI.4 Scale Height Correction Factors

Scale height factors accuracy estimates are presented in Figures 6.5 and 6.6. The first shows accuracy for the entry, or northern scales heights, while the second represents the exit, or southern scale heights.

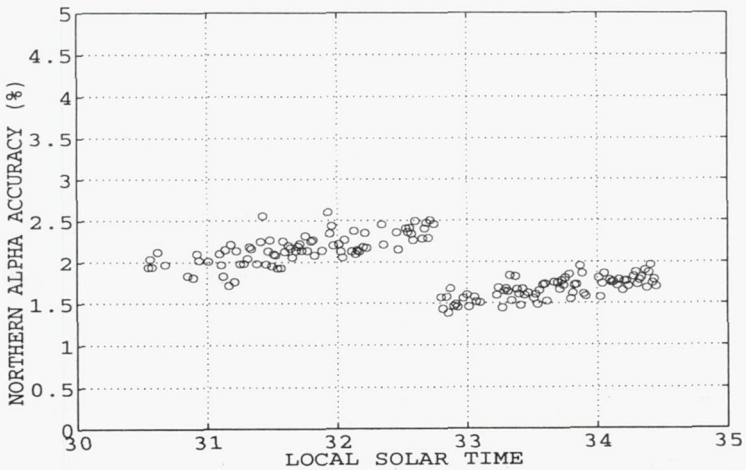

Figure 6.5 Scale Height Correction Accuracy (19° to 11° North Latitude)

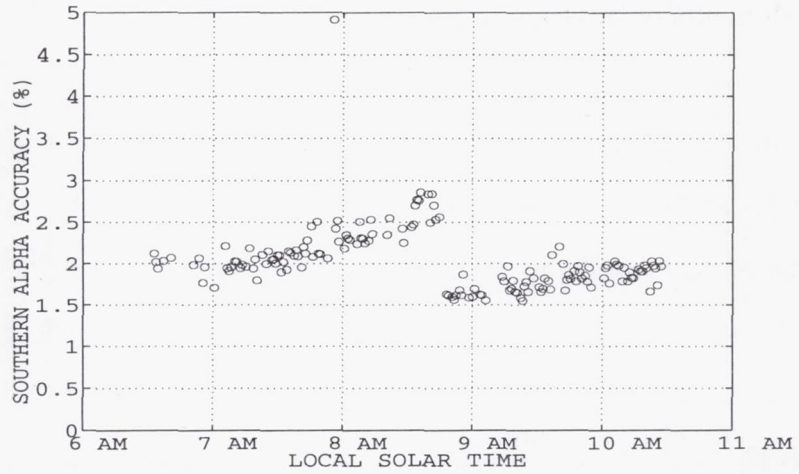

Figure 6.6 Scale Height Correction Accuracy (11° to 3° North Latitude)

Both northern and southern scale heights have normalized accuracy estimates better than 3%. Cramer-Rao bounds indicate a measurement threshold for scale height correction factors of 0.014. Again, this accuracy estimate represents the best possible measurement, i.e. no error in the Freemac pitch moment coefficient.

The non-linear nature of the scale height parameter decreases the credibility of the error estimate. In fact, this accuracy varies significantly with iteration. Error estimate may drop by more than an order of magnitude from first to final iteration. Scale height correction accuracy estimates shown in Figures 6.5 and 6.6 represent estimates for the first iteration, which are generally the worst accuracy values. Since this parameter may have considerable natural variability, the only means to confirm these error estimates is by examination of residuals. Example residuals for the scale height parameter were shown in Figures 5.6 and 5.7. Changing the scale height correction factors by 0.014, the measurement threshold indicated by the Cramer-Rao bounds, does make a small, but noticeable change in residuals.

VI.5 Mass Moments of Inertia

Estimates of accuracy associated with spacecraft bus mass moments of inertia are obtained by a statistical analysis of parameter solutions rather than from the information matrix because of the a priori conditioning requirement of the information matrix. Since the spacecraft bus moment of inertia values are nearly constant throughout Cycle Four, standard deviations are used to determine moment of inertia accuracy estimates. Table 6.1 shows measurement standard deviations and normalized accuracy. Normalized moment of inertia accuracy is obtained by dividing the standard deviation by the largest spacecraft bus moment of inertia, I_{yy}. These values represent Figures 5.14, 5.16, 5.18, 5.19, and 5.20.

Moment/Product of Inertia	Standard Deviation ($kg \cdot m^2$)	Normalized Accuracy (percent)
I_{xx}	--	--
I_{yy}	7.0	0.6
I_{zz}	4.8	0.4
I_{xy}	5.3	0.5
I_{xz}	7.1	0.6
I_{yz}	6.5	0.6

Table 6.1 Spacecraft Bus Estimated Moments of Inertia Accuracy

All mass moment of inertia values have accuracy better than 1% of the largest spacecraft bus moment of inertia. Gravity gradient effects can therefore be removed from any future tachometer measurement to better than 1%. However, since these values are all based upon the I_{xx} calibrated moment of inertia, absolute accuracy, which would be needed for rigid body motion calculations, is limited to the accuracy of the calibrated I_{xx} value. This accuracy is approximately 5%.

VI.6 Solar Moment Coefficients

Solar moment coefficient error analysis is again derived from study of the information matrix and Cramer-Rao bounds. Since all solar moment coefficients have identical partial derivatives for Eq. (13), accuracy estimates will be identical for the yaw, pitch, and roll solar coefficients. Figures 6.7 shows estimated accuracy for all three solar moment coefficients. Accuracy is plotted versus the solar longitude angle.

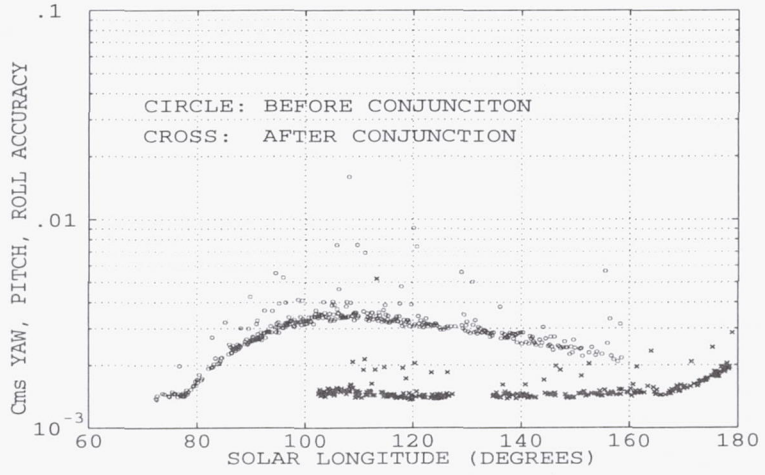

Figure 6.7 Solar Moment Coefficient Accuracy

Error as estimated by Cramer-Rao bounds are significantly better after conjunction. This variation in accuracy is the result of solar occultation. During solar occultation, there is less exposure time to solar pressure, therefore decreasing solar moment coefficient accuracy. Occultation begins at 80°, reaches a maximum at 110°, and ends at 170° solar longitude (see Figures E.8 and E.9). This corresponds with increasing, maximum, and decreasing solar moment error. Measurement threshold for a solar moment coefficients is 0.003 for periods of no solar occultation.

A statistical analysis of the estimated solar moment coefficients is done in order to verify the error model. Solar moment coefficients are partitioned into 26 groups of 25 orbits. Figure 6.8 shows the sample standard deviation of each of these groups. This figure is representative of yaw, pitch, and roll direction.

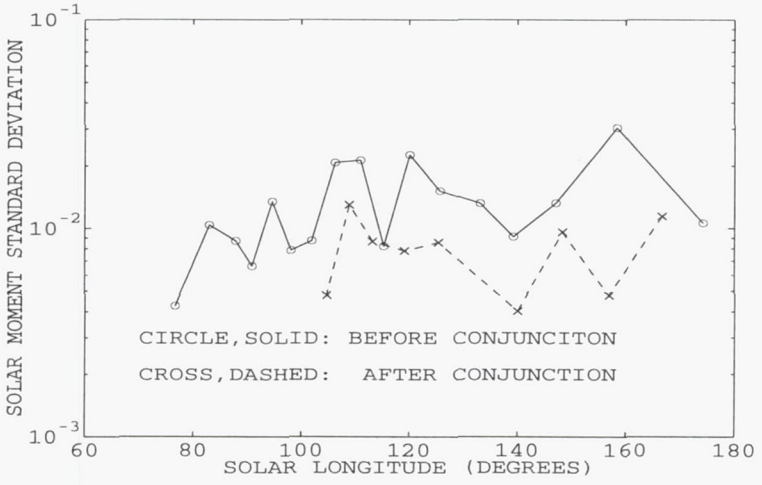

Figure 6.8 Solar Moment Coefficient Sample Standard Deviation

As with the yaw and roll aerodynamic moment coefficient, the solar moment coefficient indicates accuracy as much as ten times larger than the Cramer-Rao bounds. Again, this may be explained by the incorrect error model as describe in section VI.3.

VII. CONCLUSION

VII.1 Atmospheric

Reaction wheel data analysis has demonstrated the ability to make scientific measurements of atmospheric properties including base densities and scale heights. All atmospheric measurements required knowledge of spacecraft aerodynamics (i.e., one aerodynamic moment coefficient) as determined by free molecular flow simulations. The procedure confirmed base densities derived from orbital decay methods throughout all of Cycle Four. Accuracy estimates of base density ranged from better than 1% during the daytime to approximately 10% during the nighttime, however, error in the Freemac estimate of the pitch moment coefficient will cause additional. Cramer-Rao bounds indicated a measurability threshold for density of $8 \cdot 10^{-13}$ kg/m^3 for high rate data and $4 \cdot 10^{-12}$ kg/m^3 for low rate data. Scale heights were estimated based upon a correction to VIRA model scale heights for approximately 150 orbits late in Cycle Four. Determination of scale heights required one aerodynamic moment coefficient to be known as it varied through the atmospheric event. Measurement of scale height corrections were made separately for regions north and south of periapsis. Large scale height measurements in the more northern latitudes are inconsistent with expected values and may be due to transient accommodation coefficient effects upon the pitch aerodynamic moment coefficient.

VII.2 Aerodynamic

Two of the three aerodynamic coefficients were estimated by reaction wheel data and compared to Freemac values. The yaw aerodynamic moment coefficient showed good agreement with Freemac predictions. However, discrepancies with the roll moment

coefficient indicated a possible error in Freemac accommodation coefficient or center of mass assumptions. Error in solar array position may also contribute to error in the roll moment coefficient. Like base density, aerodynamic moment coefficient accuracy varied with local solar time. During the daytime, when atmospheric density was high, accuracy for aerodynamic coefficients was considerably lower than during nighttime local solar times.

VII.3 Mass Moments of Inertia

Five of the six spacecraft mass moments of inertia were estimated from attitude control data. Six moments of inertia could not be determined due to the linear dependent nature of the gravity gradient torque equation. Moments of inertia were modeled as the sum of contributions from the solar arrays and the spacecraft bus. Solar array moments of inertia varied as the arrays moved to follow the sun. The essentially constant spacecraft bus moments of inertia were estimated assuming a modeled variation in solar array inertia. Small deviations from constant estimates of bus moments of inertia were attributed to error in solar array inertia modeling. Spacecraft caused errors in solar array position may also have contributed to this error.

VII.4 Solar Moment Coefficients

The reaction wheel method quantified solar torques by the estimation of three solar moment coefficients. These coefficients were shown to be a function of the solar longitude and latitude within the spacecraft coordinate system. Accuracy of solar moment coefficients varied depending upon the amount of time the spacecraft was exposed to the sun. Maximum solar moment coefficient accuracy corresponded to the period of time when solar occultation was a maximum.

VIII. FUTURE WORK

A more sophisticated error model could be implemented in order to resolve the discrepancy between errors estimated by the Cramer-Rao bounds and sample standard deviations of estimated parameters. This model would take into account the dynamic friction of the reaction wheel, which causes the measurement standard deviation to be a function of reaction wheel speed.

At the end of Cycle Four, a series of aerobraking maneuvers was performed lowering the eccentricity of the Magellan orbit from 0.4 to 0.03. The end of the aerobraking phase of the mission marked the beginning of Cycle Five on August 6, 1993. Cycle Five will provide several advantages for studying the Venusian atmosphere. The more circular orbit will allow analysis of a wider atmospheric region than Cycle Four. Also, for a given altitude, the new orbit will cause the spacecraft to be within the atmosphere for a longer time. This will increase the reaction wheel method's overall sensitivity to the atmosphere. Cycle Five will also provide the opportunity to validate or improve mass moment of inertia and solar pressure torque models developed from Cycle Four analysis.

Cycle Five may present the opportunity for another scientific measurement of the Venusian atmosphere. Due to the increased time in the atmosphere, spatial variations in density due to latitudinal change may be observed. This latitudinal variation in density will have a very similar affect to scale height variation. A new method of atmospheric model parameterization must be developed to successfully separate base density, scale height, and latitudinal density variation. Cycle Five data may confirm the transient accommodation coefficient effect seen in Cycle Four scale height measurements.

Appendices

A. Reaction Wheel Speed Integral

Starting with time rate of change of angular momentum,

$$\frac{d}{dt}(\vec{H}) = \vec{T} \tag{A.1}$$

where total angular momentum of the spacecraft is defined as

$$\vec{H} = \vec{H}_{spacecraft} + \vec{H}_{rw} \tag{A.2}$$

Since the spacecraft is inertially fixed, the first term of Eq. (A.2) is zero. Each reaction wheel is positioned along one of the three orthogonal axes: yaw, pitch, and roll. Considering one of the directions and substituting Eq. (A.2) into Eq. (A.1),

$$\frac{d}{dt}(H_{rw}) = \frac{d}{dt}(I_{rw}\omega) = T \tag{A.3}$$

Note that all reaction wheels have the same moment of inertia. Integration of Eq. (A.3) gives

$$\omega = \frac{1}{I_{rw}} \int T dt + C. \tag{A.4}$$

All moments of inertia, torques, angular momentum terms are defined relative to the spacecraft center of mass.

B. Differential Correction General Equation

Define a cost function based upon residuals and a priori information as

$$2J = \vec{\varepsilon}^T \Gamma_\varepsilon^{-1} \vec{\varepsilon} + (\vec{x} - \vec{\mu}_x)^T \Gamma_x^{-1} (\vec{x} - \vec{\mu}_x) \tag{B.1}$$

where residuals, $\vec{\varepsilon}$, are defined by the observed $\vec{y}$ and the model $\vec{\omega}(\vec{x})$ as,

$$\vec{\varepsilon} = \vec{y} - \vec{\omega}(\vec{x}) \tag{B.2}$$

Minimizing the cost function yields

$$\vec{\omega}^T \Gamma_\varepsilon^{-1} \frac{\partial \vec{\omega}}{\partial \vec{x}} + \vec{x}^T \Gamma_x^{-1} = \vec{y}^T \Gamma_\varepsilon^{-1} \frac{\partial \vec{\omega}}{\partial \vec{x}} + \vec{\mu}_x^T \Gamma_x^{-1} \tag{B.3}$$

Taking transpose of Eq. (B.3) and linearizing,

$$\frac{\partial \vec{\omega}^T}{\partial \vec{x}} \Gamma_\varepsilon^{-1} \left[\vec{\omega}(\vec{x}_n) + \left. \frac{\partial \vec{\omega}}{\partial \vec{x}} \right|_n \Delta \vec{x}_n \right] + \Gamma_x^{-1} (\vec{x}_n + \Delta \vec{x}_n) = \left. \frac{\partial \vec{\omega}^T}{\partial \vec{x}} \right|_n \Gamma_\varepsilon^{-1} \vec{y} + \Gamma_x^{-1} \vec{\mu}_x \tag{B.4}$$

Note that $\partial \vec{\omega} / \partial \vec{x}$ is the sensitivity matrix A shown in Eq. (13). Rearranging terms and solving for $\Delta \vec{x}$ gives,

$$\Delta \vec{x} = \left(A^T \Gamma_\varepsilon^{-1} A + \Gamma_x^{-1} \right)^{-1} \left[\left(A^T \Gamma_\varepsilon^{-1} \vec{\varepsilon} \right) + \Gamma_x^{-1} (\vec{\mu}_x - \vec{x}_n) \right] \tag{B.5}$$

where n represents iteration number. All terms on the right-hand-side of Eq. (B.5) are evaluated at $\vec{x}_n$, and corrected parameter estimate is given by,

$$\vec{x}_{n+1} = \vec{x}_n + \Delta \vec{x}. \tag{B.6}$$

C. Model of Solar Array Mass Moments of Inertia

Solar arrays were modeled as thin plates rotating about the yaw axis. Dimension are 2.5 × 2.53 m and mass is 35 kg for each solar array. Solar array position is defined by the following figure. This example shows the solar arrays at zero degree off - point (i.e. solar array is normal to spacecraft - sun vector). However, solar array off - point may be non zero depending upon mission thermal constraints. These solar array off - points are defined as a positive rotation about the yaw axis.

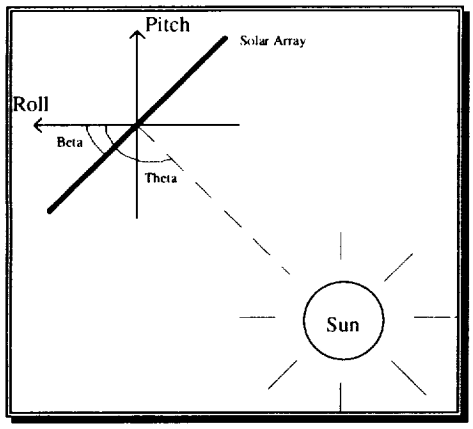

Figure C.1 Solar Array Position Definition

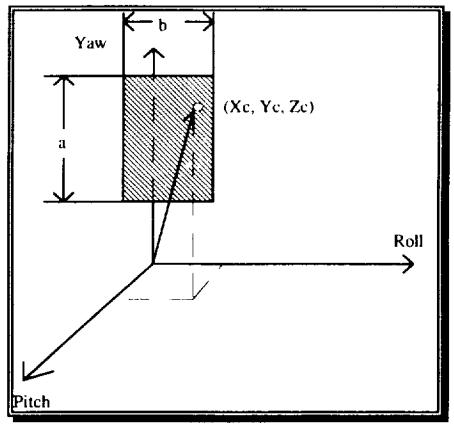

Figure C.2 Solar Array Center of Mass

Mass moments of inertia can be shown to be

$$I_{SA} = m/6 \begin{bmatrix} a^2 + 6(y_c^2 + z_c^2) & -6x_c y_c & -6x_c z_c \\ -6x_c y_c & a^2 \cos^2 \beta + b^2 + 6(x_c^2 + z_c^2) & \frac{1}{2} a^2 \sin 2\beta - 6y_c z_c \\ -6x_c z_c & \frac{1}{2} a^2 \sin 2\beta - 6y_c z_c & a^2 \sin^2 \beta + b^2 + 6(x_c^2 + y_c^2) \end{bmatrix} \quad \text{(C.1)}$$

where a = 2.53 m, b = 2.5 m, m = 35 kg, and x_C,y_C,z_C represents a general center of mass offset. Since this offset is predominately in the x (yaw) direction, y_C and z_C are both negligible in Eq. (C.1). These moments of inertia can be evaluated with the equation

$$\beta = \theta - \pi/2 \quad \text{(C.2)}$$

where the angle θ is shown in Figure E.10.

D. Magellan Attitude Control Data Analysis Software (MACDAS)

Over six thousands lines of code are used to analyze Magellan reaction wheel data. In addition, many auxiliary programs are used to supplement data manipulation and storage logistics. Code was executed on a Dell 486 50Mhz personal computer using Lahey FORTRAN. Execution time varies with number of iterations required for convergence, parameters being estimated, model time window, and time step. Solution for one orbit simulation may vary from a few seconds to minutes.

The ability to run more than one version of the program at a given time was built into MACDAS. For example, one version might be used to process scale height information late in Cycle Four at the same time as another version is processing moment of inertia parameters early in the cycle. Different version numbers prevents confusion between the output files for the user, and file sharing problems for the operating system. Actual version numbers are at the discretion of the user and is supplied through keyboard as the only manual input.

D.1 Subroutine Descriptions

The software is divided into ten modules and a driver. A brief description of all subroutines is given below.

MAGELLAN DRIVER:

Magellan: Main driver routine. Calls all subroutines.

PRELOOP1 MODULE: Subroutines used to set up run specifications

Interact:	Sets up version number for current run. Version number is used to identify files such as "pre.txt", "post.txt", "orbit.txt", "parms.par". Determine parameters to be estimated.
Manyorbits:	Specifies which orbits will be analyzed and whether a multi- or single- orbit differential correction algorithm will be employed.
Firstbaseimu:	Specify first guesses for moments of inertia, values for a priori estimates, and a priori covariance matrix standard deviations.

PRELOOP2 MODULE: Subroutine to prepare for orbit simulation

Firstlocs:	Specify first guesses for local parameter estimates.
Setorbit:	Input orbital elements from "prtsum" files.
Orbit2day:	Calculate day of year based on orbit number.
Renameparams:	Assign values of params vector to physical variable names.
Astros:	Assign preliminary constants.
Setime:	Specify time window for simulation.
Checklimits:	Assure that time window and time step does not call for more memory than current dimension statements allow.
Vme2j2k:	Convert orbital elements from Venus Mean Equator to J2000.
Gettilt:	Determine solar array off-point for given orbit.
Getpvang:	Determine solar array position based on sun, Venus, Earth position and solar array off-point.
Getipvc:	Determine model estimate of solar array moments of inertia.
Thedate:	Calls *Julian* subroutine.
Julian:	Calculates Julian date from day, month, year, etc.
Spacecraft:	Set various spacecraft specifications.
Quatern:	Calculated quaternions from solar system geometry for comparison to observed quaternions.
Getrsc2eq:	Determine transformation matrix from body-fixed spacecraft coordinate system to J2000.
Positions:	Determine Earth, Venus, sun vectors.
Getlst:	Determine local solar time.
J2k2vme:	Transform a vector from J2000 to Venus Mean Equator.
Earth:	Determine position of Earth.
Venus:	Determine position of Venus.
Getcd:	Determine Freemac estimate of Cd for given orbit.
Makebigsa:	Set up matrix containing solar array off-point information.

GET REAL MODULE: Read in reaction wheel data

Getreal:	Recover reaction wheel speeds based on orbit number and simulation time window.
Addpts:	Add points omitted from telemetry stream as dictated by data protocol.
Purgepts2:	Remove "blunder" points.
Truncate:	Assures data is within appropriate data time window.
Smoothpts:	Filter observed data. Done only after differential correction.
Lowpass:	Low pass filter used by *Smoothpts.*
Quantumrate:	Determined data rate of observed data (usually 2/3 or 20 sec).
Printrwd:	Send reaction wheel data to a file. (Used for debugging only)

LOOP MODULE: Orbit and torque simulation

Twobody:	Solves Kepler's equation.
Posandvel:	Determine position and velocity from spacecraft state.
Getsza:	Determine solar zenith angle at spacecraft periapsis location.
Dragcalc:	Model of torque due to atmospheric density.
Solar:	Model of torque due to solar pressure.
Gravity:	Model of torque due to gravity gradient.

POSTLOOP MODULE: Determine reaction wheel speeds and residuals

Convert:	Multiplies torques by time step and divides by reaction wheel mass moment of inertia.(part of integration Newton-Cotes formula)
Integrate:	Calls *sigma* and *sigma1*.
Timematch:	Interpolates model data and partial derivatives into real data time indices.
Sigma:	Integrates matrices of partial derivatives by Newton-Cotes formula.
Sigma1:	Integrates vector partial derivative with Newton-Cotes formula.
Tab:	Linear interpolation routine.
Addbias:	Adds bias to reaction wheel speeds.
Errors:	Calculates norm of residuals squared.
Residuals:	Calculates error between model and observed data.
Uncertainty:	Determines estimate uncertainty from information matrix.

CORRECTION MODULE: Differential correction subroutines

Makeata:	Assembles information matrix $A^T A$ from partial derivatives of A. Also conditions information matrix with a priori.
Makerhs:	Assembles right-hand-side vector or $A^T\varepsilon$. Also conditions right-hand-side with a priori.
Atasum:	Dot product of partial derivatives for individual element of $A^T A$.
Shrinkatarhs:	Reduces $A^T A$ and $A^T\varepsilon$ according to parameter specification.
Localfix:	Determine parameter correction for local parameters.
Updateparams:	Correct local parameter estimates with values from *Localfix*.
Partition:	Partition $A^T A$ and $A^T\varepsilon$ according to local and global parameters.
Sumparts:	Sum previous orbits and current orbit local parameter information.
Makelocals:	Assembles vector and matrix to be saved to file for multi-orbit simulations.
Globalfix:	Determines parameter correction for global parameters.
Savelocals:	Send vector and matrix determined in *Makelocals* to file.
Loadlocals:	Recover vector and matrix saved in *Savelocals*.
Fixmoments:	Correct global parameter estimates with values from *Globalfix*.
Moreorstop:	Evaluate variable used to determine if solution has converged.

VIRA2 MODULE: Venus International Reference Atmosphere (VIRA) model

Vira Constants:	Block data containing VIRA scale heights.
Vira:	Calculate density based upon base density, scale heights, and altitude.
Getwhich:	Determines which part of VIRA scale height matrix to be used as determined by local solar time.
Setbase:	Determines base altitude.

SHOWS MODULE: Screen and file output subroutines

Show1-5:	Various screen outputs for simulation status.
Show6:	File output of model data.
Show8:	File output of residuals.
Show10:	File output of observed data.
Show11:	Output to file reaction wheel speeds caused by atmospheric, gravitation, and solar torques, individually.
Foutput:	Sends data to a file, called by various *Show* subroutines.
Output:	Sends data to screen.
Showerr:	Sends residual data to files. (used for debugging only)
Showata:	File output of information matrix $A^T A$. (used for debugging only)

Showrhs:	File output of right-hand-side vector or $A^T\varepsilon$. (used for debugging only)
Gameover:	Indicates end of a successful run.
Showend:	Send parameter solutions to "end" files
Showderivate:	File output of partial derivatives of sensitivity matrix. (used for debugging only)
Writelog.	Output to "log" file various statistics of completed run.

MATRIX MODULE: Matrix manipulation toolbox

Transpose:	Transpose a matrix.
Multiply:	Multiply two matrices.
Subtract:	Subtract two matrices.
Add:	Add two matrices.
Inverse:	Invert a matrix.
Ludcmp:	LU Decomposition, called by *Inverse*.
Lubksb:	LU Back substitution, called by *Ludcmp*.

MISC MODULE: Miscellaneous mathematic and utility subroutines

Ceil:	Round up to nearest integer.
Floor:	Round down to nearest integer.
Normal:	Normalize a vector.
Cross:	Evaluate cross product.
Clearay:	Zero various matrices.
Zero:	Called by *Clearay*.
Num2string:	Convert 5 digit integer to 5 character string.
Standard:	Calculate standard deviation.
Mean2:	Calculate mean.
Monther:	Convert character representation of month to integer.
Clearscr:	Clear screen.
Dayofyear:	Determine day of year from date.
Between:	Determine angle between two vectors.
Endtoduh:	After solution convergence, moves estimates from "end" files to "duh" files.

D.2 File Interaction

Various input and output files interact with the main driver during program execution. For these explanations, question marks (?) indicate run version number. Version numbers are used to indicate a particular combination of parameters for estimation. This allows the execution of more than one program version at a given time without file usage conflict. Three x's (xxx) indicate day of year number. Five y's (yyyyy) indicate orbit number.

orbit?.txt Orbit simulation specification.

pre?.txt: Program input: Change data window time? Y/N

if yes: Start time (minutes before periapsis)

End time (minutes after periapsis)

Time step (seconds)

(return to first question)

Change data rate? Y/N

Send observed data to screen? Y/N

Send unfiltered observed data to file? Y/N

Number of filter passes?

post?.txt: Program input: Send filtered observed data to file? Y/N

Send model to data file? Y/N

Send residuals to data file? Y/N

Save log file? Y/N

Save parameter estimates to files? Y/N

parms?.par: Parameter estimate Boolean vector. (1 estimate / 0 do not estimate)

1. I_{yy}
2. I_{zz}
3. I_{xy}
4. I_{xz}
5. I_{yz}
6. cmd_{yaw}
7. cmd_{roll}
8. rho0
9. yaw bias
10. pitch bias
11. roll bias
12. cms_{yaw}
13. cms_{pitch}
14. cms_{roll}
15. scale height factor in
16. scale height factor out

cmdx,z?.end/duh	(Two files) Yaw and Roll aerodynamic moment coefficients and uncertainty.
rho?.end/duh	Base density and uncertainty (kg / m^3).
cmsx,y,z?.end/duh	(Three files) Yaw, Pitch, and Roll solar moment coefficients and uncertainty.
normx,y,z?.end/duh	(Three files) Yaw, Pitch, and Roll norm of residuals squared.
moi?.end/duh	Mass moments of inertia and uncertainties ($kg \cdot m^2$).
prod?.end/duh	Mass product of inertia and uncertainties ($kg \cdot m^2$).
base?.end/duh	Base altitude (km).
attack?.end/duh	Angles of attack: alpha and phi (rad).
iter?.end/duh	Iterations for convergence.
fin?.end/duh	Scale height correction factor and uncertainty (entry).
fout?.end/duh	Scale height correction factor and uncertainty (exit).

sh?.end/duh	Venus shadow entry and exit time (seconds since periapsis)

"end" files save values after each iteration while "duh" files only contain final estimate. Input data files are,

prtsum.xxx	Orbital elements.
rwbin.xxx	Binary reaction wheel speeds.
q4.obs	Quaternions.

Three files are used to save reaction wheel and residual data.

obsyyyyy.dat	Observed Magellan reaction wheel speed (rad/sec).
modyyyyy.dat	Model reaction wheel speed (rad/sec).
erryyyyy.dat	Residual (error) of reaction wheel speed (rad/sec).

D.3 Miscellaneous Software

The following FORTRAN (.for), Matlab (.m) and batch (.bat) files are used to supplement MACDAS software.

angles.for:	Determines various geometric parameters including orbital elements, angles of attack, Earth/Venus position, day of year, local solar time, solar array position, sun-Venus-Earth angle, inclination of the plane of the sky, solar longitude, and solar latitude.
anglesp.for	Similar to angles.for except that all values are based upon future orbital predicts.
count.for	Used to create orbit?.txt files.
lookbin.for	Used to send binary formatted rwbin.ddd to screen.

makeobs.for	Converts rwbin.ddd binary files into text files for specified time domain.
common.for	Uses VIRA scale heights to make cmdx,y,z?.end files represent base densities at a common base altitude. Requires base?.end file.
makesh.for	Calculates scale heights required to fit given base densities.
pvc.for	Generates modeled solar array mass moments of inertia.
qcal.for	Predicts quaternions.
quat.for	Extracts quaternions from quatddd.drf files.
quatsign.for	Makes signs of quaternions appropriate for interpolation.
remove.for	Removes "blunder points" from all .duh files.
rw2binb.for	Convert tach data from ASCII to binary format.
rwmake.for	Covert tach data from tachyyddd.drf format to RW.ddd format.
interpq.m	Interpolate for missing quaternions.
qp.m	Plots model, observed, and residuals for reaction wheel data.
cleanend.bat	Deletes all "end" files.

? indicates version number

yy indicates year

ddd indicates day of year

D.4 Magellan Driver Routine Flow Chart

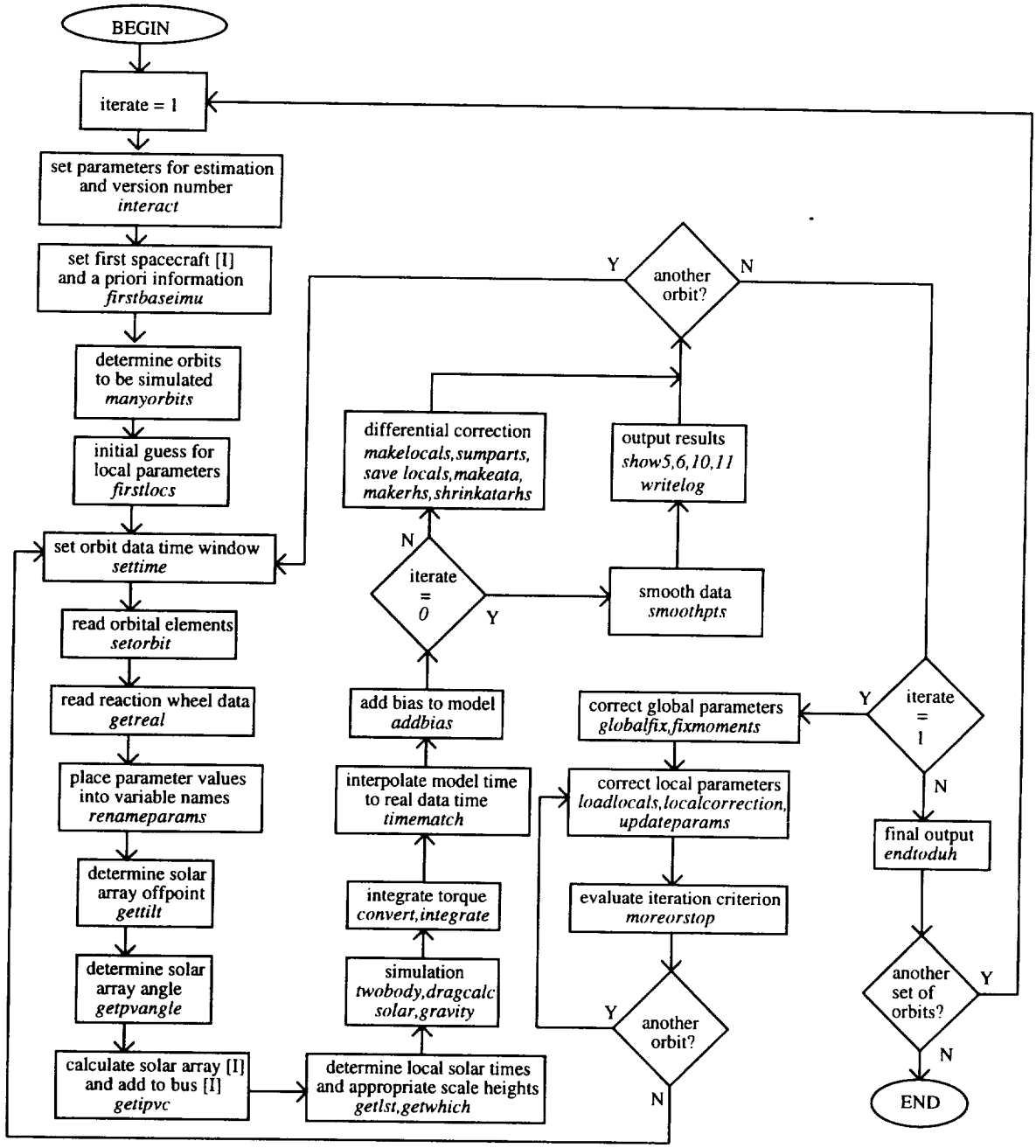

E. Cycle Four History

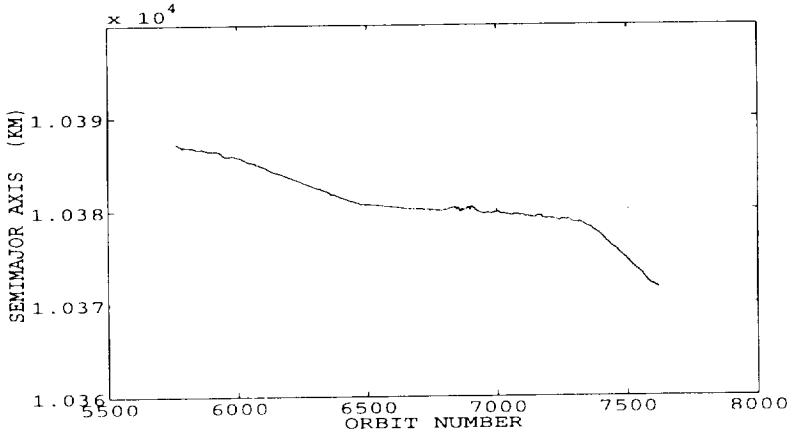

Figure E.1 Semimajor Axis

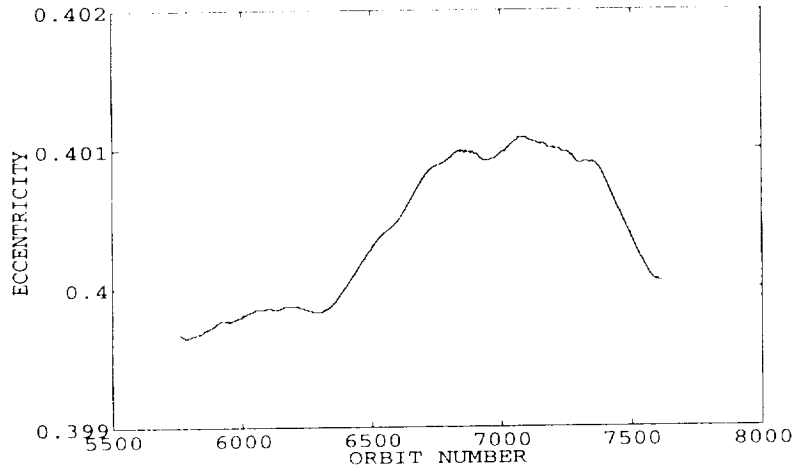

Figure E.2 Eccentricity

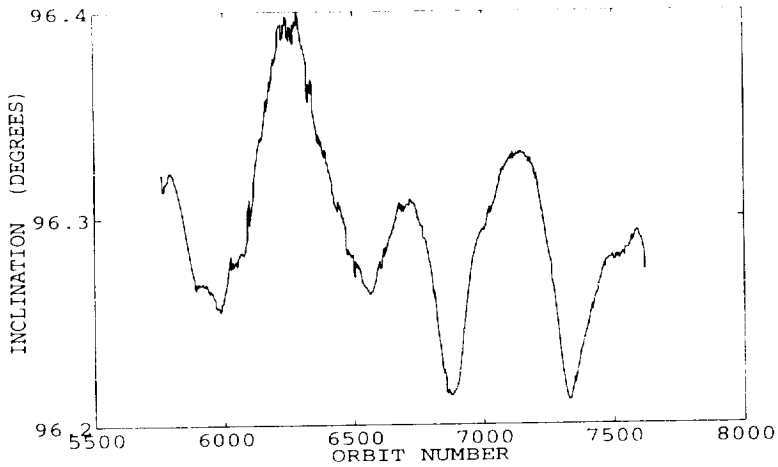

Figure E.3 Inclination (J2000)

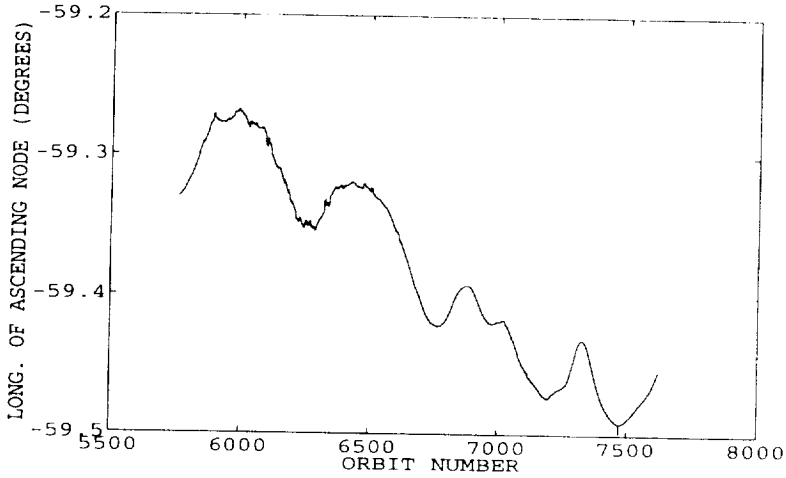

Figure E.4 Longitude of Ascending Node (J2000)

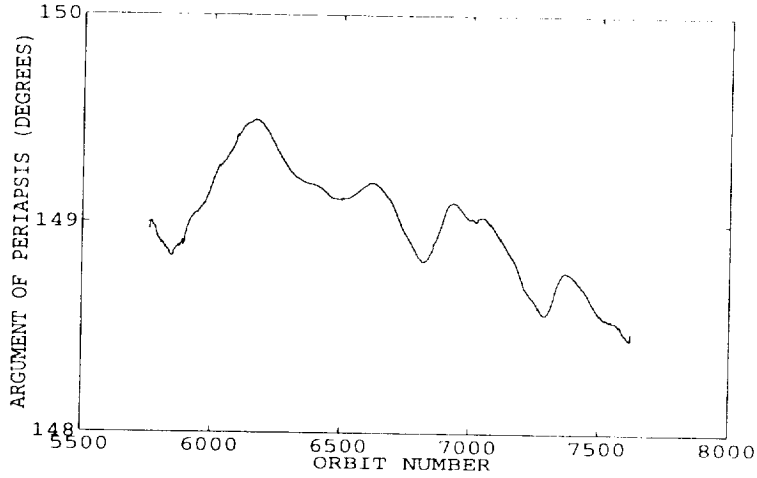

Figure E.5 Argument of Periapsis (J2000)

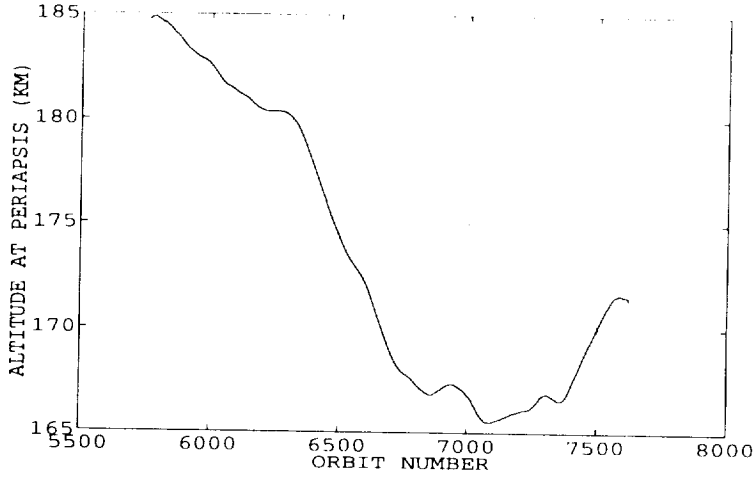

Figure E.6 Altitude at Periapsis

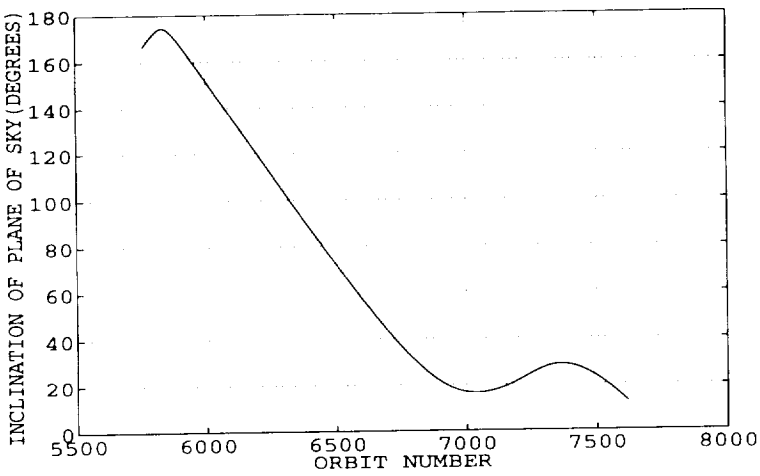

Figure E.7 Inclination of Plane of Sky

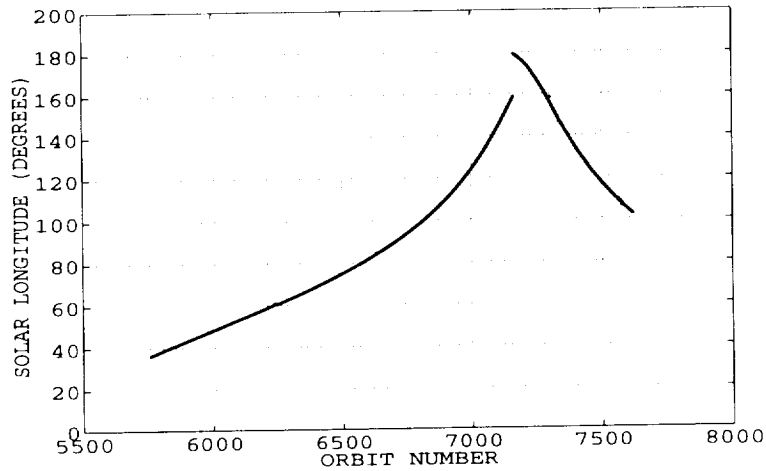

Figure E.8 Solar Longitude

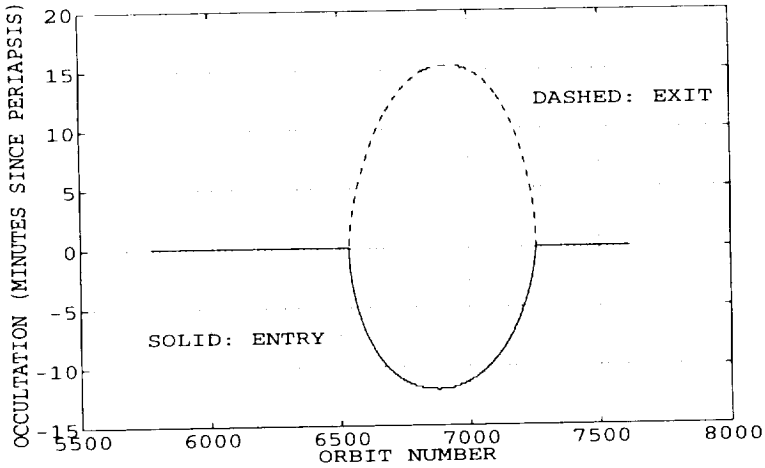

Figure E.9 Solar Occultation

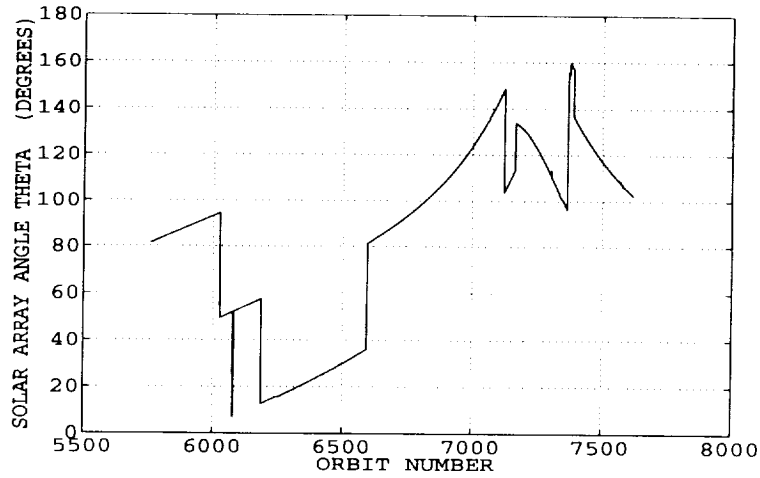

Figure E.10 Solar Array Angle Theta

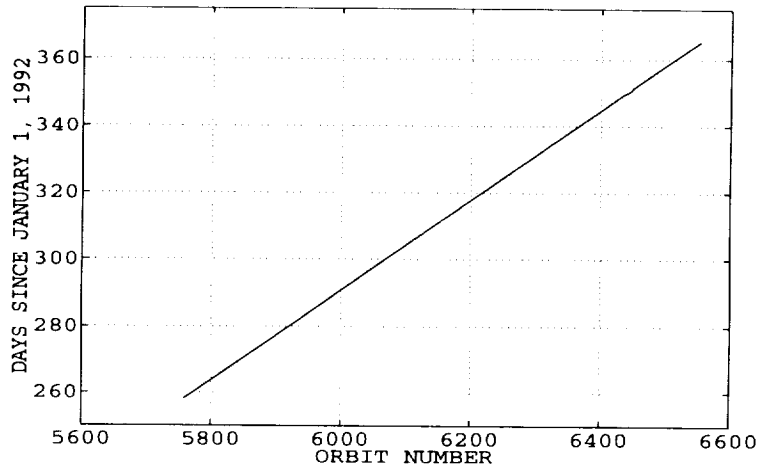

Figure E.11 Orbit Number and Day of Year (1992)

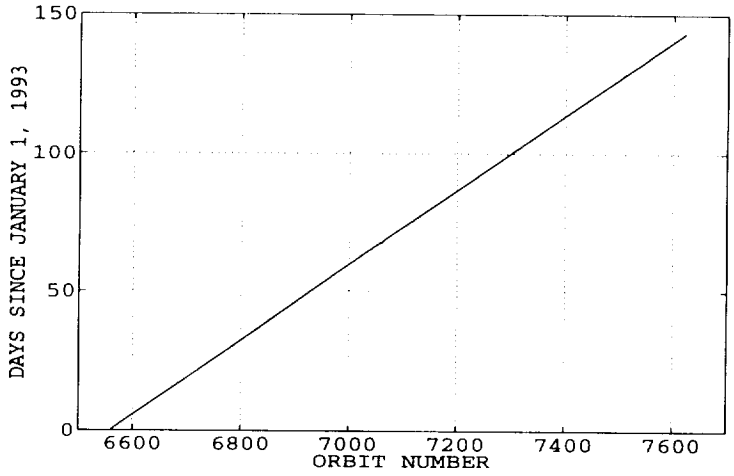

Figure E.12 Orbit Number and Day of Year (1993)

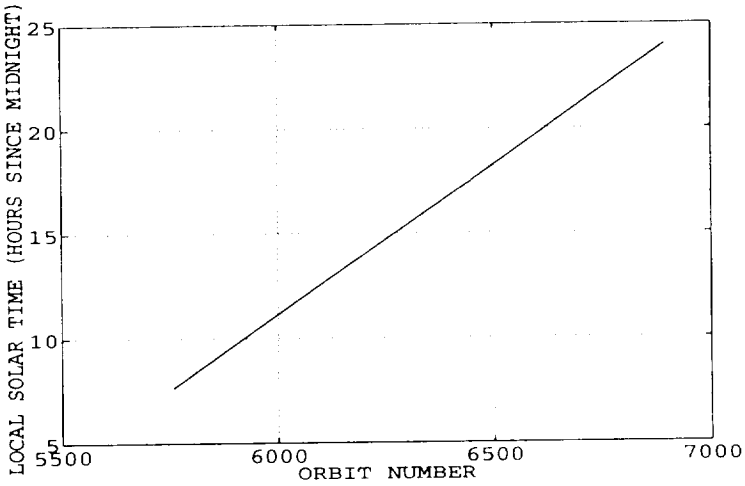

Figure E.13 Orbit Number and Local Solar Time

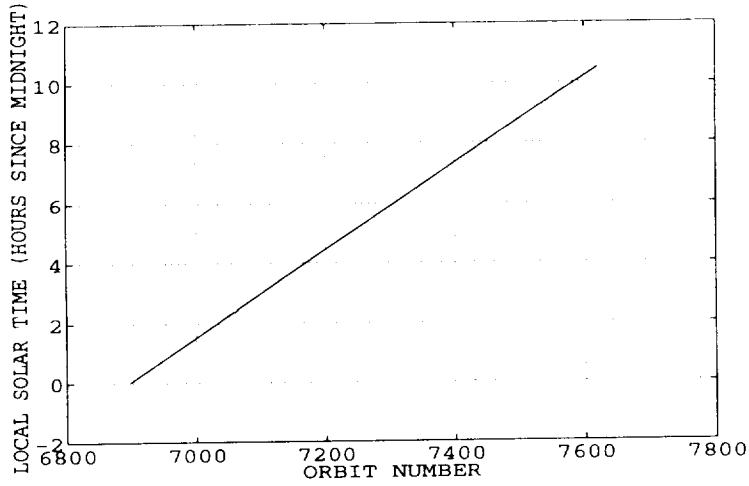

Figure E.14 Orbit Number and Local Solar Time

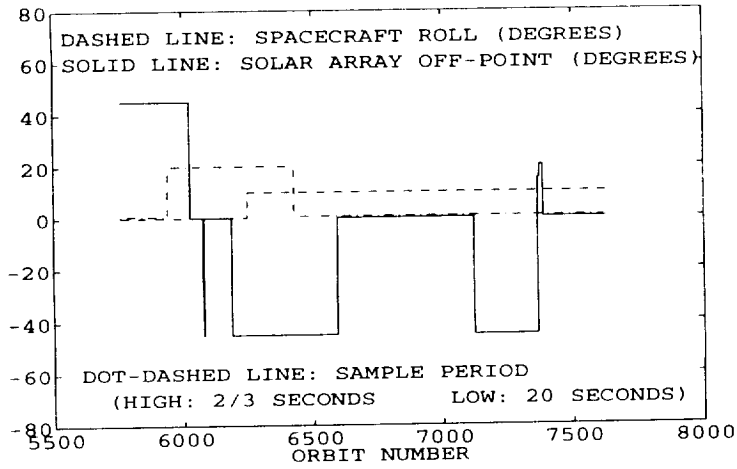

Figure E.15 Spacecraft Roll Angle, Solar Off-Point Angle, Data Rate

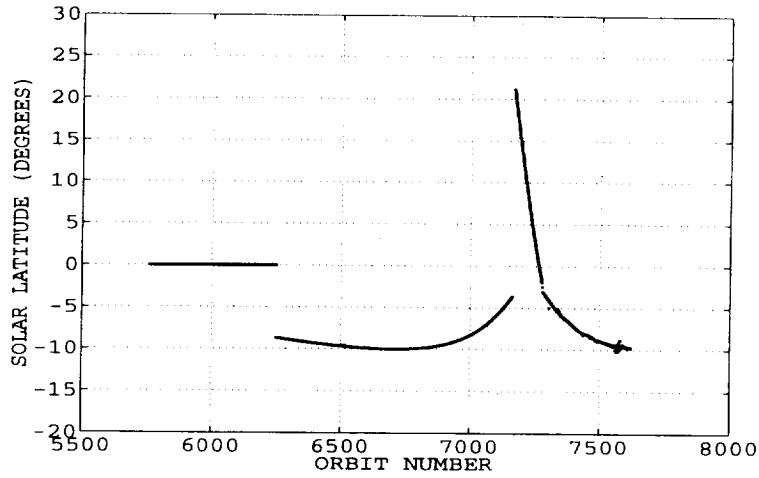

Figure E.16 Solar Latitude

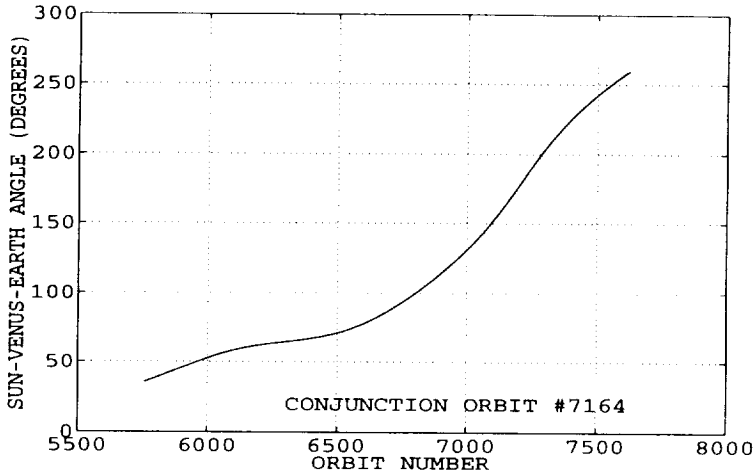

Figure E.17 Sun-Venus-Earth Angle

F. Reaction Wheel Data Logistics

Data required for reaction wheel analysis is stored on VAX/VMS workstation at the Jet Propulsion Laboratory in Pasadena, California. This data includes prtsum (orbital elements), quat (quaternions), and tach (reaction wheel speeds) files. In general, each file represents data for one Earth day, and therefore contains information for approximately eight Magellan orbits. Files are copied to an intermediate VAX/VMS machine at the NASA Langley Research Center and then transferred to a personal computer. Before this information can be processed by the MACDAS software, some pre-processing must be performed for the tach and quat files.

Tach files are placed on a Langley VAX/VMS computer using the filename TACHyyddd.DRF, where yy is 92, 93, or 94, and ddd represents the day of year. The program *makerw.for* removes unwanted characters from the TACHyyddd.DRF file and places results in the file RW.ddd. This ASCII file contains time and three reaction wheel speeds. A second program called *rw2binb.for* converts the ASCII file into binary as the file RWBIN.ddd. The binary formatted file is the observed reaction wheel speed input file for MACDAS. Both RW.ddd and RWBIN.ddd are backup up using a tape drive system. Cycle Five data has the designation RW5.ddd and RWBIN5.ddd for reaction wheel files.

Quat files also required pre-processing before use with MACDAS. Since quaternions (spacecraft attitude) change very little for each orbit, it is only necessary to know and store the quaternions for the instant of periapsis rather than the entire orbit. The program *quat.for* is used to search QUATddd.DRF for the quaternions that represent spacecraft attitude near periapsis. Again, ddd represents day of year. In order to find the correct quaternions within a particular QUATddd.DRF file, the time of periapsis must be know. This information is retrieved by the quat program from the appropriate PRTSUM.ddd file. Output from the *quat.for* program is a file containing orbit numbers

and corresponding quaternions. For a few orbits, quaternions are not found within QUATddd.DRF files. These missing values may be determined from an interpolation between known quaternions since the changes in spacecraft attitude (at periapsis) are gradual. The Matlab program *interpq.m* is used to perform this interpolation. Care must be take to correctly interpolate these quaternions since an attitude does not uniquely determine a set of quaternions. That is, a sign change of all quaternions does not alter spacecraft attitude. The program *quatsign.for* may be used to insure that signs are such that the interpolation will be done correctly. The final data file for quaternions is Q?.OBS, where ? is either 4 for Cycle Four, or 5 for Cycle Five. This file contains orbit numbers and quaternions for each orbit near periapsis which is used by MACDAS.

PRTSUM.ddd files require no special pre-processing before use with MACDAS.

References

1. D. King-Hele, *Satellite Orbits in an Atmosphere: Theory and Applications,* Blackie, 1987.

2. H. Curtis, "Magellan: Aerobraking at Venus," *Aerospace America*, vol. 32, no. 1, pp. 32-36, January 1994.

3. D. Lyons, "Aerobraking Magellan: Plan versus Reality," AAS-94-118, American Astronautical Society / American Institute of Aeronautics and Astronautics Space Flight Mechanics Meeting, Cocoa Beach, Florida, February 1994.

4. P. Marsden and C. Croom, "Determining Atmospheric Density and Spacecraft Aerodynamic Properties from Magellan Attitude Data," American Institute of Aeronautics and Astronautics Mid-Atlantic Regional Student Conference, Annapolis, Maryland, April 1993.

5. P. Marsden, "Determining the Atmospheric Density of Venus and Magellan Aerodynamic Properties from Spacecraft Attitude Data," M. S. Thesis, The George Washington University, June 1993.

6. C. Croom and R. Tolson, "Using Magellan Attitude Data to Study Venusian Atmosphere and Various Spacecraft Properties," AAS-94-141, American Astronautical Society / American Institute of Aeronautics and Astronautics Space Flight Mechanics Meeting, Cocoa Beach, Florida, February 1994.

7. G. M. Keating, A. J. Kliore, and V. I. Moroz, "Venus International Reference Atmosphere," *Advances in Space Research*, vol. 5, No. 11, 1985.

8. D. T. Lyons, "Magellan: Planetary Constants and Models," JPL D-2300, Rev. E, April 1, 1992, sect. 2-1.

9. D. T. Lyons, "Magellan: Planetary Constants and Models," JPL D-2300, Rev. E, April 1, 1992, sect. 2-22.

10. National Aeronautics and Space Administration, Magellan: *The Unveiling of Venus.* JPL 400-345 3/89, March 1993, pp. 23.

11. D. Doody, "Magellan Mapping Update: A Matter of Gravity," *Aerospace America,* vol. 31, no. 5, May 1993, pp. 20-24.

12. R. Fredo and M. Kaplan, "Procedure for Obtaining Aerodynamic Properties of Spacecraft," AIAA-81-4214, *Journal of Spacecraft,* vol. 18, no. 4, July-August, 1981.

13. L. Meirovitch, *Methods of Analytical Dynamics,* McGraw-Hill, New York, 1971, pp.437.

14. D. Marguardt, "An Algorithm for Least Squares Estimation of Nonlinear Parameters," *Journal of SIAM*, vol. 2, 1963, pp. 431-441.

15. R. E. Maine, K. W. Iliff, "Identification of Dynamic Systems," AGARD-AG-3000, 1984, ch.11.

16. G. M. Keating, N. C. Hsu, "The Venus Atmospheric Response to Solar Cycle Variations," *Geophysical Research Letters*, vol. 20, No. 23, December 1993, pp. 2752-2754.

17. D. T. Lyons, "Magellan: Planetary Constants and Models," JPL D-2300, Rev. E, April 1, 1992, sect. 8-3.

REPORT DOCUMENTATION PAGE

Form Approved
OMB No 0704-0188

1. AGENCY USE ONLY (Leave blank)	2. REPORT DATE	3. REPORT TYPE AND DATES COVERED
	August 1994	Contractor Report

4. TITLE AND SUBTITLE
Venusian Atmospheric and Magellan Properties From Attitude Control Data

5. FUNDING NUMBERS
NCC1-104
889-62-00-01

6. AUTHOR(S)
Christopher A. Croom
Robert H. Tolson

7. PERFORMING ORGANIZATION NAME(S) AND ADDRESS(ES)
Joint Institute for Advancement of Flight Sciences
The George Washington University
Langley Research Center
Hampton, VA 23681-0001

8. PERFORMING ORGANIZATION REPORT NUMBER

9. SPONSORING/MONITORING AGENCY NAME(S) AND ADDRESS(ES)
National Aeronautics and Space Administration
Langley Research Center
Hampton, VA 23681-0001

10. SPONSORING/MONITORING AGENCY REPORT NUMBER
NASA CR-4619

11. SUPPLEMENTARY NOTES Langley Technical Monitor: Lawrence F. Rowell
The information presented in this report was offered by the first author as a thesis in partial fulfillment of the requirements for the Degree of Master of Science, The George Washington University, JIAFS, Hampton, Virginia.

12a. DISTRIBUTION/AVAILABILITY STATEMENT
unclassified - unlimited

subject category 46

12b. DISTRIBUTION CODE

13. ABSTRACT *(Maximum 200 words)*

Results are presented of the study of the Venusian atmosphere, Magellan aerodynamic moment coefficients, moments of inertia, and solar moment coefficients. This investigation is based upon the use of attitude control data in the form of reaction wheel speeds from the Magellan spacecraft. As the spacecraft enters the upper atmosphere of Venus, measurable torques are experienced due to aerodynamic effects. Solar and gravity gradient effects also cause additional torques throughout the orbit. In order to maintain an inertially fixed attitude, the control system counteracts these torques by changing the angular rates of three reaction wheels. Model reaction wheel speeds are compared to observed Magellan reaction wheel speeds through a differential correction procedure.

This method determines aerodynamic, atmospheric, solar pressure, and mass moment of inertia parameters. Atmospheric measurements include both base densities and scale heights. Atmospheric base density results confirm natural variability as measured by the standard orbital decay method. Potential inconsistencies in free molecular aerodynamic moment coefficients are indentified. Moments of inertia are determined with a precision better than 1% of the largest principal moment of inertia.

14. SUBJECT TERMS
aeronomy, spacecraft aerodynamics, Magellan, Venusian atmosphere attitude control

15. NUMBER OF PAGES
96

16. PRICE CODE
A05

17. SECURITY CLASSIFICATION OF REPORT	18. SECURITY CLASSIFICATION OF THIS PAGE	19. SECURITY CLASSIFICATION OF ABSTRACT	20. LIMITATION OF ABSTRACT
unclassified	unclassified	unclassified	